FACULTY OF SCIENCE AND TECHNOLOGY

MASTER'S THESIS

Study programme / specialisation: Environmental Engineering Water Science and Technology	Spring semester, 2023 Open
Author: Hazel Margrethe Perrens	Hazel M Perrens (Writer's signature)
Supervisor at UiS: Roald Kommedal External supervisor(s): Per Møller-Pedersen Storm Aqua	
Thesis title: Hydraulic Behaviour: A Tracer Study of a Stormwater Detention and Sedimentation System	
Credits (ECTS): 30	
Keywords: Stormwater treatment Sedimentation Tracer study Hydraulic behaviour Mixing Rhodamine WT	Pages: 80 + appendix: 8 Stavanger, *14/02/2023*

Hydraulic Behaviour: A Tracer Study of a Stormwater Detention and Sedimentation System

University of Stavanger

Hazel Margrethe Perrens

February 2023

Acknowledgements

To start, I would like to thank Per Møller-Pedersen at Storm Aqua AS for allowing me the opportunity to take part in their work with stormwater treatment solutions. His dedication and enthusiasm for alleviating the consequences of urbanization and climate change has kept me inspired throughout the process. To Lars Møller-Pedersen; it has been a true pleasure to work with you. Thank you for all the practical help, equipment setup and not to mention invaluable discussions and feedback when I felt stuck. In addition, a huge thanks to Geir Lillebø for assistance during field experiments and making sure I didn't have to get my hands dirty by climbing down manholes and into treatment tanks.

Furthermore, I want to thank my future employer, Offshore Norge, for providing me with an office place in a productive environment to ensure I made it to the finish line. To Hans Kristian Brekken: thank you for your assistance with laboratory related work and technical instrument support.

I would like to especially thank my supervisor, Assoc. Prof. Roald Kommedal. Thank you for keeping me motivated throughout the study programme, and for your ideas, help and guidance with this thesis. I will never forget your reply when I knocked on your office and asked if you had time: "No, but come on in!".

Finally, a special thanks to my husband, Marten, for your patience and continuous support throughout my years of studying. Your encouragement has kept my eyes on the price. Thank you for getting me through this without losing my marbles.

Abstract

Stormwater is of growing concern with increased heavy rainfall and runoff surfaces from urbanisation. The challenges of stormwater has two aspects; risk of flooding and risk of pollution. Road runoff in particular, can at times transport a cocktail with hydrocarbons, heavy metals and other pollutants which could be detrimental to the environment of receiving water bodies.

One way to manage these challenges is by sending water through stormwater detention tanks. In Sandnes, Norway, the road runoff from a new highway is lead through an underground modular settling system (MSS), which serves the purpose of both water detention and pollutant removal by sedimentation. Established guidelines are in place for the function of water detention, but design for optimal treatment is based on a "Best Available Technology" principle.

The treatment performance of stormwater detention tanks is highly influenced by hydraulic characteristics, such as hydraulic residence time, mixing and short-circuiting. Longitudinal mixing and short-circuiting may reduce the treatment performance. In this thesis, a tracer study is applied to characterize these hydraulic processes.

Four analysis methods were selected from literary findings: (1) Visual inspection of tracer curves, (2) Method of moments (MOM) technique (3) Tank-in-series (TIS) and laminar convection flow (LCF) modelling and (4) Volume-based residence time analysis for variable flow. From the analysis, the hydraulic parameters of flow regime, mean residence time, dispersion, mixing scale and tracer mass recovery found that the hydraulic behavior of the MSS involved moderate amounts of deadzones, relatively high mixing and possibly multiple flow paths. The findings suggest the design of the MSS can be further improved to optimise hydraulic behavior for particle settling. The results should be treated with caution, however, as a statistical analysis was not possible due to practical limitations for replication tests. In addition, outflow rate had to be estimated by calculations due to instrumental errors for flow measurements. Additional studies should be done to validate the findings of this thesis, by the use of proper outflow measurements. Future tracer studies should be paired with an analysis of particle removal to better understand how hydraulic behavior and removal efficiency relates to each other and how they are influenced by different design configurations.

Contents

Acknowledgements i

Abstract ii

List of figures vii

List of tables viii

Abbreviations ix

List of symbols x

1 Introduction 1

2 Theory 2
2.1 Stormwater . . . 2
2.2 Gravity Separation Theory . . . 3
2.2.1 Discrete particle settling . . . 4
2.2.2 Particle Settling Velocity . . . 5
2.2.3 Residence time . . . 7
2.2.4 Stormwater particles . . . 8
2.2.5 Treatment efficiency of sedimentation . . . 8
2.3 Hydraulic characterization . . . 8
2.3.1 Design considerations for stormwater detention tanks . 9
2.3.2 Tracer studies . . . 10
2.3.3 Analysis of the residence time distribution . . . 11
2.3.4 Laminar and turbulent flow . . . 13
2.3.5 Convection model of laminar flow . . . 14
2.3.6 Method of moments analysis . . . 16
2.3.7 Tank-in-series modelling . . . 19
2.3.8 Non-steady state analysis . . . 20
2.3.9 Qualitative tracer curve analysis . . . 22
2.3.10 Influence of hydraulic behavior on settling efficiency . . 22
2.4 Rhodamine WT as a tracer in aquatic tracer studies . . . 23
2.4.1 Properties Rhodamine WT . . . 24
2.4.2 Rhodamine WT as tracer for sedimentation tank analysis 28
2.4.3 Fluorescence: Instrumental analysis of RWT . . . 28
2.5 Thesis Objective . . . 31

3 Methods **33**
3.1 Site description . . . 33
3.2 Materials . . . 34
3.2.1 Chemicals . . . 34
3.2.2 Analytical instrument . . . 34
3.2.3 Flowmeter . . . 34
3.3 Tracer study setup . . . 36
3.3.1 Experiment 1 . . . 36
3.3.2 Experiment 2 . . . 37
3.3.3 Tracer injection . . . 38
3.3.4 Water samples . . . 38
3.3.5 Estimation of flow and volume . . . 40
3.4 Data analysis . . . 41
3.4.1 Method of moments . . . 41
3.4.2 Volume-based RTD . . . 42
3.4.3 Models and curve fitting . . . 42
3.4.4 Sedimentation analysis . . . 42
3.4.5 Statistical analysis . . . 42

4 Results and discussion **45**
4.1 Methodological evaluation . . . 45
4.1.1 Regression analysis and limit of detection . . . 45
4.1.2 Validation of calibration curve . . . 46
4.2 Tracer study setup . . . 47
4.2.1 Experiment 1 . . . 47
4.2.2 Experiment 2 . . . 47
4.2.3 Operational conditions . . . 48
4.3 C-curves and qualitative analysis . . . 51
4.4 Method of moments analysis . . . 53
4.5 Model curves . . . 54
4.6 Volume-based RTD analysis . . . 56
4.7 Influence of hydraulic behavior on sedimentation . . . 57
4.8 Limitations of this study . . . 59
4.9 Suggestions for future studies . . . 60

5 Conclusion **61**

References **63**

6 Appendix **71**

Appendix **71**

List of Figures

2.1 Definition sketch of an ideal horizontal flow sedimentation tank with discrete particle settling, modified from Tchobanoglous et al. (2014, p. 351). 4
2.2 A sphere settling in a liquid: Flow producing a drag force F_d and falling by gravity F_g as shown in Kommedal (2020). . . . 6
2.3 A tracer study setup for experimentally determining the tracer response curve for a pulse tracer injection, adapted from Tchobanoglous et al. (2014, p. 1360) and EPA (1986). . . 11
2.4 Definition sketch of ideal reactors and their respective tracer response curves: (a)CFSTR and (b)PFR as illustrated in Tchobanoglous et al. (2014, p. 25). 12
2.5 Decision-making tree for choosing hydraulic modelling technique from Stephenson and Sheridan (2021). 13
2.6 Flow types in a pipe, categorized as (a) Laminar flow and (b) Turbulent flow. 14
2.7 Four combinations of tracer input and output measurement from (Levenspiel, 1999, p.342). 14
2.8 Tracer response curves for laminar flow in pipes. The different output curves change depending on various tracer input and output measurement, retrieved from Kommedal (2022). 15
2.9 C-curves of misbehaving plug flow reactors from Levenspiel (1999, p. 288), (a) correct mean, (b) mean too early, (c) multiple decaying peak, (d) double peaks and (e) late curve. . 22
2.10 Example of non-ideal flow conditions in a PFR, as illustrated in Tchobanoglous et al. (2014, p. 1932). 23
2.11 RWT released at Imperial Beach, California. Clark et al. (2014) used RWT to study dispersion and transport in the surfzone near shore. 25
2.12 Fluorescence principle of the TAL-PC sensor. Retrieved from YSI webinar series (Smith, 2019). 29
2.13 Temperature-correction curves for RWT and other tracer dyes, as seen in Wilson et al. (1986). 30

3.1 Technical drawing from Storm Aqua AS (2021). 33

3.2 Schematics of the tracer study setup at the MSS at Fv505, Sandnes. The pump was used for experiment 1, but not experiment 2. Position of tracer injection point and YSI sensor remain the same for both experiments. Modified from Storm Aqua AS (2021). 37
3.3 Schematic illustration of EXO1 sonde mounted in outlet pipe from settling tank 1. 38
3.4 YSI sonde secured to steel bar. 39
3.5 Terms for a partially filled, horizontal cylinder. 41

4.1 Calibration curve with fluorescence, RFU, plotted against standard concentrations of Rhodamine WT, $\mu g/L$. 46
4.2 Depth data from YSI-sensor during Experiment 1, with illustrated times for pump switch, full tank (overflow) and no pump. 50
4.3 Flow curve, with Q_{in} and Q_{out} plotted versus time. 50
4.4 Tracer output curve, or C-curve, for Experiment 1. 52
4.5 Tracer output curve, or C-curve from Experiment 2. 52
4.6 Tracer response curve fitted with model curves: $C(t)_{F,F}$, $C(t)_{F,P}$, $C(t)_{P,P}$ and the TIS-model. The peaks of $C(t)_{F,F}$ and $C(t)_{P,P}$ are cutoff from the plot due to very high values (>3000 ug/L). 56

6.1 Calibration curve with fluorescence, RFU, plotted against standard concentrations of Rhodamine WT, $\mu g/L$ 71
6.2 Pump setup for experiment 1 - The pump (a) was lowered into tank 3 with a rope, and the cable transported water out from tank 3 (b) 74
6.3 Pump setup for experiment 1 - The cable had to be positioned to avoid angles for smooth flowthrough (a) of water into inlet chamber (b) 74
6.4 YSI probe setup for sampling 75
6.5 Selected tracer study data from Experiment 1 and calculated parameters for volume-based RTD analysis. 76
6.6 Selected tracer study data from Experiment 1 and calculated parameters for assumed steady-state MOM-analysis 77
6.7 Selected tracer study data from Experiment 1, model data from TIS and LCF models and calculations for sum of squared errors with input mean residence time, τ, from Excel SOLVER function. 78

All figures without direct attribution are self-made.

List of Tables

2.1 Term descriptions for particle settling theory equations as given in Tchobanoglous et al. (2014). 7
2.2 Physio-chemical properties of RWT (National Center for Biotechnology Information, 2022; Skjolding et al., 2021; Tai & Rathbun, 1988). 24
2.3 Predicted no effect concentration (PNEC) and estimated environmental quality standards (EQS) of RWT (National Center for Biotechnology Information, 2022; Skjolding et al., 2021). 26

3.1 Equations for reactor analysis with method of moments technique and the volume-based RTD approach. 43
3.2 Functions and equations used for LCF and TIS-modelling. . . 44

4.1 Regression analysis of calibration curve. 45
4.2 Validation results. 47
4.3 Calculated operational conditions for Experiment 1 and 2. . . 48
4.4 Hydraulic characteristics from Experiment 1, MOM. 55
4.5 Zeroth (M_0^*), first (M_1^*) and second moment (M_2^*) , followed by the moment index (MI) from the volume-based RTD analysis. 57
4.6 Calculation terms and resulting settling velocity (υ_p) and settling time (t_s). 58

6.1 Regression analysis of calibration curve. 71
6.2 Standard RWT solutions for analysis (C_2) with dilution volumes and concentrations. 73

Abbreviations

The following abbreviations of standard phrases are used throughout the thesis.

Abbreviation	Meaning
AA-QS	Annual-average quality standard
CFSTR	Continuous Flow Stirred Tank Reactor
EQS	Environmental Quality Standard
Fv 505	Fylkesvei 505
HRT	Hydraulic retention time
LCF	Laminar Convection Flow
MAC-QS	Maximum allowable concentration quality standard
MOM	Method of Moments
MSS	Modular Settling System
NIVA	Norwegian Institute of Water
NPRA	Norwegian Public Roads Administration. Nor: Statens Vegvesen
PNEC	Predicted no effect concentration
RTD	Residence time distribution
RWT	Rhodamine WT
TAL-PC	Total Algae Phycocyanin Smart Sensor
TIS	Tank-in-series
TSS	Total Suspended Solids

List of symbols

The following table presents standard notations and units used throughout the thesis.

Symbol	Description	Unit
A	Catchment Area	m^2
A_I	Accuracy Index for Tracer mass recovery	unitless
A_p	Cross-sectional area of particle	m^2
C_d	Drag coefficient	unitless
C_f	Climate factor	unitless
$C_0 = \frac{M_i}{V}$	Initial tracer concentration	$\mu g/L$
$C(t)$, $C_{out}(t)$	Outlet tracer concentration at time t	$\mu g/L$
$C(\phi)$	Normalised concentration at flow-weighted time	unitless
d	dispersion number	unitless
D	Dispersion coefficient	m^2/s
d_p	Diameter of particle	m
e	Effective volume ratio	unitless
F_g	Gravitational force	N
F_d	Drag force	N
F_b	Buoyant force	N
g	Acceleration due to gravity	m/s^2
H	Water depth	m
HRT	Hydraulic Residence time	min
I	Precipitation intensity	$L/s \cdot ha$
L	Length of reactor	m
λ	Hydraulic efficiency	unitless
M_0^*	Normalised zeroth moment	unitless
M_1^*	Normalised first moment	unitless
M_2^*	Normalised second moment	unitless
M_{out}	Total recovered tracer mass	g
MI	Moment Index	unitless
N	Number of CFSTR tanks-in-series	unitless
P_e	Peclet number	unitless
Q_{dim}	Dimensioning flow for design	m^3/s
Q_{out}	volumetric outflow rate	m^3/s
N_R	Reynolds number	unitless
R	Hydraulic radius/characteristic length	m
ρ_p	Particle density	kg/m^3
ρ_w	Water density	kg/m^3
sg_p	specific gravity of the particle	unitless

σ_c^2	C-curve variance	min^2
σ_θ^2	Dimensionless variance	unitless
t	Time after tracer injection	min
dt	Time difference of sample frequency	min
t_s	Settling time	min
t_m	Mean residence time	min
t_n	Nominal residence time	min
t_p	Time of peak concentration	min
tau	Residence time for LCF and TIS model	min
V_m	mass averaged volume	m^3
V_P	Volume of particle	m^3
V_{sys}	System volume (constant)	m^3
$V_t(t)$	Time averaged volume at time t	m^3
$V(t)$	System volume at time t	m^3
υ_p	Particle settling velocity	m/s
υ	fluid velocity	m/s
μ	Dynamic viscosity	$N \cdot s/m^2$
ν	Cinematic viscosity	m^2/s
ϕ	Flow weighted time	unitless
φ	Runoff coefficient	unitless

1. Introduction

Stormwater management has traditionally had one purpose: To reduce the hydrological load with flood control systems such as detention tanks. These are designed to capture the stormwater temporarily, before gradually releasing it at controlled rates to the downstream drainage system (Ødegaard, 2014). Stormwater detention tanks have become progressively urgent due to increased high intensity rain events caused by global warming (UN-Water, 2019). In addition to flood risks, stormwater is also a significant source of pollution. Road runoff in particular has shown to contain heavy metals, hydrocarbons and fuel additives which can have serious consequence to the quality of receiving water bodies (Hoffman et al., 1985; Li et al., 2008). Consequently, the treatment of road runoff has received increased attention. Stormwater detention tanks can have a pollution control function, as they provide time for particle removal by sedimentation (Nix, 1985).

Design guidelines for detention tanks are well established, but there is a lack of guidelines for treatment optimisation. Ideally, sedimentation is designed according to a minimal hydraulic residence time (HRT) which allow particles of interest enough time to settle (Tchobanoglous et al., 2014). With steady-state conditions, residence time is defined as volume divided by flow rate, providing a relatively simple design criteria. However, the incidental nature of rainfall events with the ensuing dynamic flow rate and variable volume complicates the process (Nix, 1985).

This thesis is part of a research project seeking to improve treatment of road runoff through a multistage concept (Research Council of Norway, 2019). As part of the project, an underground modular settling system (MSS) was built with the multipurpose of detention and treatment of roadway runoff from a new highway in Sandnes, Norway. The thesis work of Bergseng (2021) and Gausel Lode (2021) tested for particle removal efficiency at various rainfall events, with results in the range of 48-98% removal of total suspended solids (TSS).

Removal efficiency is influenced by the hydraulic behavior within the system. System design affects mixing and short-circuiting which again influence the HRT. These characteristics are commonly described experimentally by the use of inert tracers thought to track the movement of water through the system. Various methods and calculations are applied to analyse a tracer study (Headley & Kadlec, 2007). In this project a full scale tracer study will be executed and results analysed in order to provide experimental understanding of hydraulic behavior and actual residence time in stormwater detention tanks.

2. Theory

The following chapter will provide a theoretical background relevant for the thesis. First, an introduction about the challenges with stormwater runoff is presented, followed by an overview of sedimentation theory and hydraulic characterisation of treatment reactors. Then, the general principles of designing a tracer study for hydraulic characterisation is described. Lastly, the objective of the thesis is stated.

2.1 Stormwater

In Norway, stormwater management is well integrated into project planning of new roads and infrastructure (NPRA, 2018). Traditionally, the main strategy has been to lead runoff water to surface infiltration areas, into stormwater pipes or a combined sewer system. Heavy rainfall events along with increased runoff surfaces from urbanisation, has led to challenges in volume capacity for existing water management systems. In addition, stormwater runoff could have a detrimental effect on the environment in receiving water bodies (Hoffman et al., 1985). Roadway runoff can at times be highly contaminated with pollutants such as road salt, hydrocarbons, fuel additives, particles from tyres and a range of heavy metals (Marsalek et al., 2003; Westerlund & Viklander, 2006). This cocktail of organic and inorganic contaminants can disturb aquatic ecosystems. Meland (2010) demonstrated how pollution from roadway runoff had harmful biological effect in sea trout (*Salmo trutta*).

These concerns regarding stormwater runoff are addressed by Norwegian law in the Norwegian Water Regulation (Vannforskriften, 2006), with the intent to secure a good ecological and chemical status for aquatic environments. The regulations are implemented in road design through the Norwegian Public Roads Administration (NPRA) handbook N200, whereby treatment is based on the vulnerability of receiving water body and annual average daily traffic (NPRA, 2018).

During the road design of Fv 505, a regional highway in Sandnes, it became clear that road runoff had to be treated before entering the Figgjo river system. Serving as a nature reserve for birds, a salmon spawning location and a home for rare river mussels, the Figgjo river system is considered of high ecological importance (Ledje & Randulff, 2019). In order to maintain a healthy salmon population, the river system has been granted protection status through Norwegian law (Innst. S. nr. 183 (2006-2007), n.d.), which means that any activity or intervention which could harm the salmon population or the water environment is prohibited. The river is also recognized internationally

through the Ramsar convention, which is an international cooperation for the protection of wetlands that are important for species diversity, nesting and wintering areas for migratory birds. Although agriculture runoff is considered the largest environmental challenge for the river, a recent report also highlighted runoff from construction activities and future urbanization as a major pollution contributor to the Figgjo river system (Ledje & Randulff, 2019).

The MSS is installed as a step to relieve roadway runoff pollution from Fv 505 and serves as the test site for this thesis.

2.2 Gravity Separation Theory

The MSS is designed to achieve both flood and pollution control of the stormwater runoff from Fv505. Detention serves as a volume storage to reduce overflows to the receiving water system, and the treatment step applies sedimentation to separate particles from the stormwater runoff. Sedimentation is involved in almost all treatment methods for roadway runoff, where suspended particles heavier than water are physically separated from water through gravitational settling (Åstebøl & Hvitved-Jacobsen, 2014; Droste & Gehr, 2019). The following section will describe some fundamental sedimentation principles, to illustrate how the HRT will influence treatment efficiency of gravitational settling.

Sedimentation theory can be roughly divided into four types (Tchobanoglous et al., 2014, p. 345):

I. Discrete settling - particles settle as individual entities

II. Flocculent settling - Particles coalesce and increase in mass, which in turn increases the settling rate

III. Hindered settling - Particles remain in fixed position relative to each other, and settle as a unit

IV. Compression settling - High concentrations of particles make up a structure which settles by compression

Findings by Li et al. (2005) suggest that particles grow in a settling tank, as described by Type II settling. However, in order to keep calculations simple and conservative, the same authors used discrete settling theory when studying optimization of settling tank design (Li et al., 2008). In NPRA guidelines, the assumption of discrete settling is also advised for roadway runoff treatment design (Åstebøl & Hvitved-Jacobsen, 2014). Thus, this thesis will also assume discrete settling in the MSS.

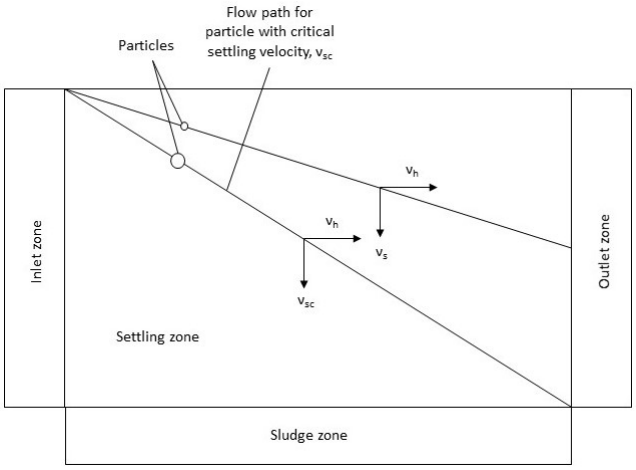

Figure 2.1: *Definition sketch of an ideal horizontal flow sedimentation tank with discrete particle settling, modified from Tchobanoglous et al. (2014, p. 351).*

2.2.1 Discrete particle settling

As described above, discrete settling occurs when each particle settle individually by gravity, without any significant interaction with other, surrounding particles (Tchobanoglous et al., 2014). Figure 2.1 shows a definition sketch of ideal discrete particle settling in a horizontal flow, rectangular sedimentation basin. The inlet and outlet zones are also a part of the sedimentation length, but high turbulence is assumed near the entrance with no settling. Similarly, with flow streamlines towards the exit which at times flow upward, no settling is assumed in the outlet zone. For wastewater treatment, a sedimentation tank is designed by selecting a particle with a critical settling velocity, ν_{sc}. This is the minimum settling velocity needed for a particle to settle through the entire depth of the tank during the HRT of the system. HRT is described by Tchobanoglous et al. (2014) as "the time a unit volume of water is in the basin". All particles with a settling velocity equal to or greater than ν_{sc} is removed, while particles with a lower settling velocity, such as ν_s in Figure 2.1, may exit with the effluent, depending on settling zone entry height. Droste and Gehr (2019) present some other important assumptions for ideal discrete settling:

1. Water and particles entering the inlet zone is dispersed uniformly, resulting in the same suspended solids (SS) concentration across the entire depth of the inlet zone.

2. Steady-state conditions with constant flow rate.

3. HRT equals the flow through period, meaning ideal hydraulic conditions with no dead space or short-circuiting of water volume (see Section 2.3).
4. Plug flow conditions (see Section 2.3).
5. Particles settle individually, i.e discrete settling.
6. No movement of liquid in the sludge zone.

2.2.2 Particle Settling Velocity

All equations in this section are reproduced from the material of Tchobanoglous et al. (2014, p. 346-349) and Kommedal (2020), and all terms are described in Table 2.1 at the end of this section.

With respect to discrete settling, Newtons gravitational law and Stoke's drag law can be used to calculate particle settling velocity. Figure 2.2 shows how a spherical particle settling in a liquid is governed by gravitational force, F_g and drag force, F_d by the liquid. In addition, a buoyant force upward, F_b is exerted on the particle by the liquid. At terminal critical settling velocity, the sum of forces is given as:

$$\sum F = F_g - F_b - Fd = 0 \tag{2.1}$$

F_g, F_b and F_d are described by the following equations:

$$F_g = \rho_p V_p g \tag{2.2}$$

$$F_b = \rho_w V_p g \tag{2.3}$$

$$F_d = \frac{C_d A_p \rho_w \upsilon_p^2}{2} \tag{2.4}$$

Solving for particle settling velocity, ν_p, yields:

$$\nu_p = \sqrt{\frac{4gd_p}{3C_d}\left(\frac{\rho_p - \rho_w}{\rho_w}\right)} \approx \sqrt{\frac{4gd_p}{3C_d}(sg_p - 1)} \tag{2.5}$$

Equation 2.5 show that the diameter and density of a particle determine its settling velocity (Droste & Gehr, 2019). The shape of the particle affects the drag coefficient and spherical particles will be assumed for the purpose of this thesis.

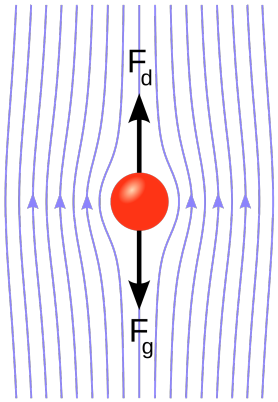

Figure 2.2: *A sphere settling in a liquid: Flow producing a drag force F_d and falling by gravity F_g as shown in Kommedal (2020).*

The drag coefficient also depends on the flow regime around the particle. Reynolds number, N_R, is used to distinguish if the flow is laminar ($N_R < 1$), transitional ($N_R = 1$ to 2000) or turbulent ($N_R > 2000$). For spherical particles, the drag coefficient is given by the following equation:

$$C_d = \frac{24}{N_R} + \frac{3}{\sqrt{N_R}} + 0.34 \tag{2.6}$$

For the different flow regimes, the drag coefficient is approximated to:

$$Laminar \rightarrow C_d = \frac{24}{N_R} \tag{2.7}$$

$$Transition \rightarrow C_d = \frac{24}{N_R} + \frac{3}{\sqrt{N_R}} + 0.34 \tag{2.8}$$

$$Turbulent \rightarrow C_d = 0.4 \tag{2.9}$$

By identifying the flow regime, and thus applying the correct drag coefficient, the particle settling velocity can be determined. In laminar conditions, viscosity is the principal force, and settling velocity, v_p is given by Stoke's equation:

$$v_p = \frac{g(\rho_p - \rho_w)d_p^2}{18\mu} \approx \frac{g(sg_p - 1)d_p^2}{18\nu} \tag{2.10}$$

When the flow regime is transitional, C_d from Equation 2.8 must be used in its entirety in Equation 2.5 to determine v_p.

Table 2.1: *Term descriptions for particle settling theory equations as given in Tchobanoglous et al. (2014).*

Term	Description	Unit
ρ_p	Particle density	kg/m^3
ρ_w	Water density	kg/m^3
V_P	Volume of particle	m^3
g	Acceleration due to gravity	m/s^2
C_d	Drag coefficient	unitless
A_p	Cross-sectional area of particle	m^2
υ_p	Particle settling velocity	m/s
d_p	Diameter of particle	m
sg_p	specific gravity of the particle	unitless
μ	Dynamic viscosity	$N \cdot s/m^2$
ν	Cinematic viscosity	m^2/s

For turbulent flow conditions, inertial forces are predominant and a value of 0.4 is used as C_d, and settling velocity is calculated from the following equation:

$$\upsilon_p = \sqrt{3.33g\left(\frac{\rho_p - \rho_w}{\rho_w}\right)d_p} \approx \sqrt{3.33g(sg_p - 1)d_p} \tag{2.11}$$

2.2.3 Residence time

The main purpose of a sedimentation tank, such as the MSS, is to trap particles inside the tank. In essence, a particle is trapped when the time needed for sedimentation is equal to or shorter than the retention time. The time, t_s required for a given particle with diameter d_p on the water surface to settle to the bottom of the tank is equal to the ratio (Raimondi & Becciu, 2017):

$$t_s(d_p) = \frac{H}{\upsilon_s(d_p)} \tag{2.12}$$

where H is the water depth and $\upsilon_s(d_p)$ is the settling velocity of a particle with diameter d_p. The critical settling velocity and basin depth is related to HRT as such (Tchobanoglous et al., 2014, p. 350):

$$\nu_{sc} = \frac{H}{HRT} \tag{2.13}$$

Throughout this thesis, HRT is expressed as either nominal (theoretical V/Q) or mean residence time, t_n or t_m respectively.

2.2.4 Stormwater particles

Organic pollutants, heavy metals and suspended solids are the primary pollutants of urban runoff . Other pollutants of concern are the nutrients nitrogen and phosphorus, pathogenic microorganisms and road salt (Åstebøl & Hvitved-Jacobsen, 2014). This thesis will mainly concern the suspended solids which the MSS is designed to remove. By properly characterising the influent particles from Fv 505, settling velocity may be calculated. Previous case studies of the MSS provide some insight on influent particles in the stormwater from Fv 505 (Bergseng, 2021; Gausel Lode, 2021). With the objective of assessing treatment efficiency, both studies also applied particle size distribution (PSD) analysis, in which a distribution of particle diameters were determined.

Gausel Lode (2021) found that 90% of particles were smaller than 8 μm. Bergseng (2021) evaluated the removal efficiency of the MSS with respect to TSS larger than 0.45 μm, and reported results of 48%, 92% and 98%. The lowest efficiency was reported for the highest flow into the MSS, and Bergseng (2021) noted that increased incoming volume decreases the time for settling. For particles with low settling velocity, there is not enough time for settling (Li et al., 2008).

Hydraulic retention time will be one of the parameters used for hydraulic characterisation in this thesis. As found by Bergseng (2021), the HRT will vary according to inflow conditions, but the resulting HRT for the given test conditions can be compared to stormwater particle settling time.

2.2.5 Treatment efficiency of sedimentation

In short, treatment efficiency of a sedimentation tank depends on the range of particle settling velocities and the hydraulic retention time. The flow regime and mixing in the system influence the hydraulic retention time, which makes hydraulic characterisation important in order to improve system design and efficiency.

2.3 Hydraulic characterization

The previous section demonstrated how treatment efficiency of a sedimentation tank depends on the range of particle settling velocity and hydraulic retention time. The mixing regime influences the hydraulic retention time and is important to characterize. Understanding a reactors hydraulic behavior has great influence on stormwater detention tank design for optimizing treatment

efficiency. The standard norm for stormwater detention tank design is volume-based for flood protection. A report by Åstebøl and Hvitved-Jacobsen (2014) for the NPRA, provide some recommendations with respect to treatment of roadway runoff. The report highlights that treatment efficiency is connected to the hydraulic conditions in the basin. Factors such as hydraulic retention time, energy conditions by the inlet, laminar or turbulent flow regime, and risk of sediment erosion are all mentioned in the report. Hydraulic conditions depend on the dimensions of the system, which makes design considerations crucial for effective treatment. In this thesis, the experimental procedures and analysis described below will be used to characterize the hydraulics of the MSS.

2.3.1 Design considerations for stormwater detention tanks

Design criteria for wastewater sedimentation tanks are well established. Tchobanoglous et al. (2014) mention HRT, overflow rate, scour velocity (to avoid re-suspension of sediments) and the characteristics and quantities of solids as important design considerations. For stormwater detention tank design, however, the main design criteria is to ensure sufficient detention volume for the increased stormwater load. Detention works as storage and gradual release of stormwater runoff. When planning new urban establishments, roads and infrastructure, increased stormwater load is accounted for through predicted precipitation of catchment area, runoff coefficients and a climate factor. In Norway, these considerations are thoroughly described in norms set by the municipality offices (Norsk Vann, 2020). This is also the case for the design of the MSS. For catchment areas smaller than 20 ha, Norsk Vann (2020) and Ødegaard (2014, p. 346) provide the following equation for stormwater management design, known as the rational equation:

$$Q_{dim} = \varphi A I C_f \tag{2.14}$$

where Q_{dim} is dimensioning flow for design, φ is the runoff coefficient, I is the precipitation intensity from IVF-curves specific to the area, A is the catchment area and C_f is the climate factor. Runoff coefficients estimate how much of the precipitation will become surface runoff, and is based on the infiltration characteristics of the surface area. Dense surfaces, such as asphalt roads and buildings, have high values approaching 1, while green surfaces such as parks and forests have coefficients between 0.3 and 0.5 (Norsk Vann, 2020). IVF-curves uses historical precipitation data to estimate how

often a precipitation event with a given intensity and duration will happen for the the selected area. According to Norsk Vann (2020), the area for the MSS facility falls within a frequency of a 20 year return period and a 10-min duration. The frequency and duration is used to identify an intensity of 186.4 L/s·ha from the IVF-curve representative of the area. With a standard climate factor of 1.2, design intensity is 223.68 L/s·ha (Storm Aqua AS, 2021). By using the rational equation, Storm Aqua AS (2021) calculated the runoff to increase from 96.5 L/s to 265.7 L/s with the construction of Fv505. The increased runoff load constitutes a minimum detention volume of 115 m^3 at the MSS. Calculation details are provided upon request from Storm Aqua AS. For particle removal purposes, the dimensions of the MSS are designed according to recommendations from the NPRA report by Åstebøl and Hvitved-Jacobsen (2014), but details of the design process is classified as company confidentiality information and cannot be provided (L. Møller-Pedersen, personal communication, December 20, 2022).

Åstebøl and Hvitved-Jacobsen (2014) explain design principals for effective sedimentation in pond systems, but guidelines are not as detailed as for water detention design. Furthermore, the report points out that stormwater treatment design is not defined by established water quality standards, but rather by indirect standards from "Best Available Technology". In the stormwater management municipality norm of eigth pages (Norsk Vann, 2020), only two sentences are dedicated to treatment of stormwater: "Generally, there are no requirements for stormwater treatment. If the stormwater is significantly polluted, efforts to reduce pollutant discharge should be established and clarified with the municipality office". The MSS in Sandnes is partly funded by The Research Council of Norway, through a project called "New multistage concept for treatment of road water", with the objective of improving "Best Available Technology" for stormwater treatment (Research Council of Norway, 2019).

2.3.2 Tracer studies

Different reactor types can be used to describe flow and hydraulics. Two examples of reactor types are plug flow reactors (PFR) and complete-mix reactors, commonly referred to continuous flow stirred tank reactor (CFSTR) (Levenspiel, 1999; Tchobanoglous et al., 2014). These represent two extremes of mixing conditions, but most reactors have conditions somewhere in between. To better understand hydraulic behavior in reactors, scientists and engineers use residence time distribution curves (RTD), obtained from tracer studies. According to a report by the U.S Environmental Protection Agency, tracer studies are considered "the most reliable and efficient method" for analysis

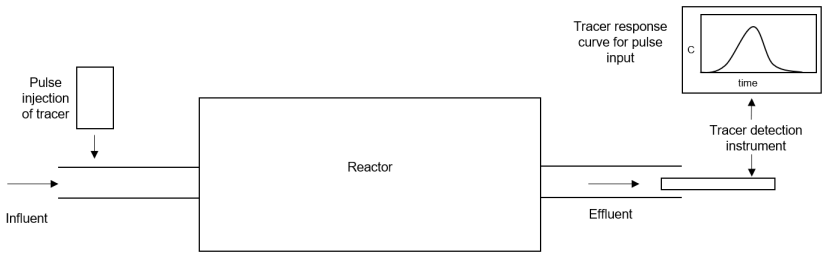

Figure 2.3: *A tracer study setup for experimentally determining the tracer response curve for a pulse tracer injection, adapted from Tchobanoglous et al. (2014, p. 1360) and EPA (1986).*

of surface and subsurface hydraulic systems (EPA, 2002). Principally, an aquatic tracer study is performed by adding a tracer, such as a dye or other chemical, to the inlet pipe of the system, and measuring the tracers arrival in the effluent continuously for a given period of time. Measurements can be made by collection series of grab samples or instrumental methods. The measurements result in a tracer test response curve, known as the C-curve, and is plotted as exit concentration versus time. A C-curve is commonly normalized to produce an RTD curve, often referred to as an E-curve, for further analysis (Tchobanoglous et al., 2014). Figure 2.3 shows a tracer study setup for a pulse injection of tracer, with the resultant C-curve.

2.3.3 Analysis of the residence time distribution

RTD analysis for reactor characterization was first introduced by Danckwerts (1953). Analytical tools for interpreting flow-regimes mainly distinguish between the PFR and CFSTR (Levenspiel, 1999). An ideal CFSTR, shown in Figure 2.4a, will achieve instantaneous mixing across the entire reactor as water enters. With steady-state conditions, the RTD is characterized by an exponential decaying curve. Ideal PFRs on the other hand, have minimal longitudinal mixing and are associated with high length-to-width ratio tanks as illustrated in Figure 2.4b. In a PFR, water and its dissolved constituents travel uniformly from inlet to outlet, with no dispersion (Tchobanoglous et al., 2014).

In practice, reactors seldom have ideal flow conditions. Non-ideal flow analysis is done by evaluating how far it deviates from the ideal situation (Levenspiel, 1999). Headley and Kadlec (2007) state that the degree of non-ideality is mainly driven by velocity profiles and mixing. Figure 2.4 also

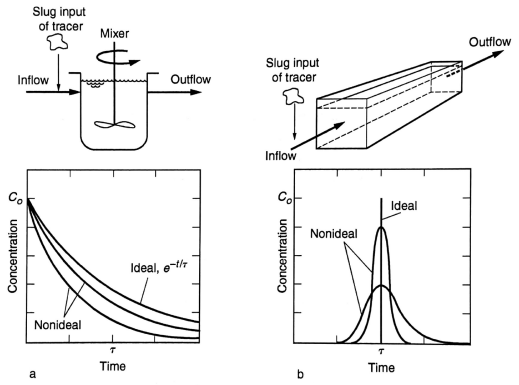

Figure 2.4: *Definition sketch of ideal reactors and their respective tracer response curves: (a)CFSTR and (b)PFR as illustrated in Tchobanoglous et al. (2014, p. 25).*

shows the C-curve obtained from a tracer study. For the PFR, the ideal output response shows how effluent tracer concentration should be equal to the influent concentration C_0. The HRT, occurring at the concentration peak, should be equal to the theoretical detention time (Tchobanoglous et al., 2014). Nonideal PFR C-curves are shown as bell-shaped curves, ie. Gaussian distribution, due to axial dispersion, as shown in Figure 2.4b.

Steady-state is an important assumption for the ideal PFR flow regime, whereby inflow is equal to outflow, and constant over time. Analytical methods for RTD analysis of variable flow patterns have been proposed in several studies, especially in the field of constructed wetlands (Werner & Kadlec, 1996). Although the MSS is not a constructed wetland, it serves the same purpose for water treatment and detention. For analysis purposes, constructed wetlands are thought of as treatment reactors, which makes the hydraulic analysis method relevant for systems such as the MSS.

In a recent review, Stephenson and Sheridan (2021) present various techniques and models for tracer study analysis in constructed wetlands for stormwater treatment. The review offers a guide for investigating and modelling hydraulic characteristics, presented as a decision-making tree shown in Figure 2.5. According to this guide, the method of moments (MOM) and the tank-in-series (TIS) model are appropriate techniques for characterising the hydraulic of the MSS. In addition, the convection model of laminar flow(LCF) from Levenspiel (1999) may be useful. The TIS and LC are both examples of modelling the tracer response curve. Essentially, modelling is a curve fitting practice. The objective is to produce a model which best portray the tracer response curve for the tested system. The preceding techniques for analysis are further elucidated in the sections to

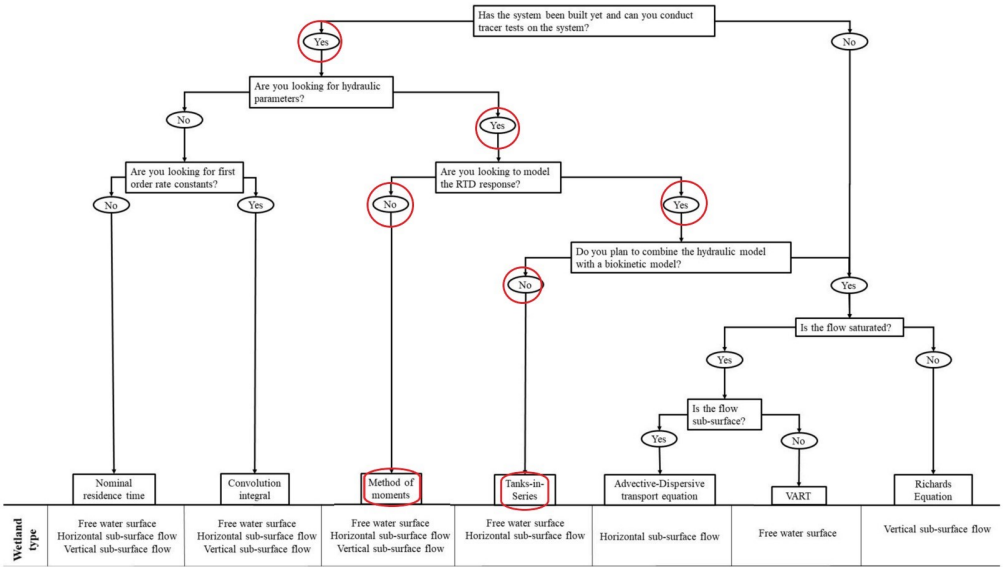

Figure 2.5: *Decision-making tree for choosing hydraulic modelling technique from Stephenson and Sheridan (2021).*

follow, after a brief distinction of laminar and turbulent flow regimes.

2.3.4 Laminar and turbulent flow

As mentioned previously, types of flow is often categorized as either turbulent or laminar. The flow regime is influenced by the resistance of flow, which is determined by Reynolds number, N_R (Tchobanoglous et al., 2014):

$$N_R = \frac{\upsilon R}{\nu} \tag{2.15}$$

which shows how water velocity, υ, hydraulic radius, R, and kinematic viscosity, ν influences the local velocity profile through the cross sectional area of a pipe. Equation 2.15 assumes full pipe flow conditions, while the following equation accounts for open-channel flow where water flows with a free surface:

$$N_R = \frac{4\upsilon R}{\nu} \tag{2.16}$$

with terms defined previously.

Laminar flow is preferred for effective sedimentation (Åstebøl & Hvitved-Jacobsen, 2014). Laminar flow occurs at low velocities, where the fluid is

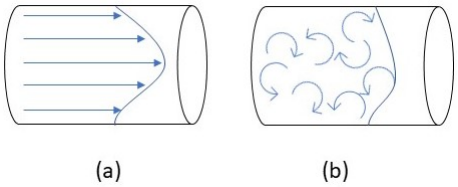

Figure 2.6: *Flow types in a pipe, categorized as (a) Laminar flow and (b) Turbulent flow.*

thought to be sectioned in parallel layers, without lateral mixing. Layers towards the middle of the pipe has a higher velocity than layers closer to the pipe wall, as seen in Figure 2.6a.

Turbulent flow normally has higher velocity. Fluid velocity is thought to continuously change direction and magnitude, as seen in Figure 2.6b.

As stated in Section 2.2 the following ranges of N_R determine the flow regime: Laminar flow ($N_R < 1$), transitional flow ($N_R = 1$ to 2000) and turbulent flow ($N_R > 2000$). Various engineering resources report different limit values for flow regimes, but a N_R below 2000 is generally accepted as laminar flow conditions (Engineering ToolBox, 2004).

2.3.5 Convection model of laminar flow

In an ideal PFR, all fluid particles move through the reactor with the same velocity, and have the same HRT. When the flow regime is laminar, fluid particle velocities are distributed with a parabolic profile as shown in Figure 2.6a, with fastest flowing fluid in the center. The response curve of an ideal laminar plug flow is highly dependent on how tracer is introduced into the fluid and how it is measured, which are divided into flux and planar introduction and/or measurement. These are shown as four combinations in Figure 2.7.

Levenspiel (1999) introduces a convection model for laminar flow, where each fluid velocity from the parabolic profile present an individual residence time as shown in the RTD in Figure 2.8. Flux conditions apply when the

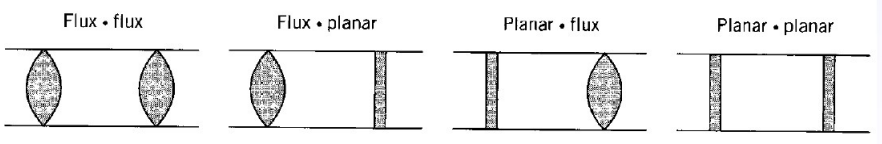

Figure 2.7: *Four combinations of tracer input and output measurement from (Levenspiel, 1999, p.342).*

tracer concentration is centered in the cross-sectional area. If the tracer is evenly distributed over the cross-sectional area, planar conditions apply (Levenspiel, 1999).

Modelling exit curves from laminar convection flow

The modified equations on the next page are used to model the C-curves of the different input-output combinations (Kommedal, 2022; Levenspiel, 1999, p. 343). These can be further used to compare and fit to C-curves from tracer data, as means to estimate the hydraulic residence time, shown as τ in the equations. τ will be comparable to t_m, mean residence time, from measured tracer data.

$$C(t) = \frac{M_i}{V} \cdot \frac{\overline{\tau}^3}{2t^3} \tag{2.17}$$

for Flux_{in} to Flux_{out}.

$$C(t) = \frac{M_i}{V} \cdot \frac{\overline{\tau}^2}{2t^2} \tag{2.18}$$

for Flux_{in} to $\text{Planar}_{out}t$ and Planar_{in} to Flux_{out}.

$$C(t) = \frac{M_i}{V} \cdot \frac{\overline{\tau}}{2t} \tag{2.19}$$

for Planar_{in} to Planar_{out}.

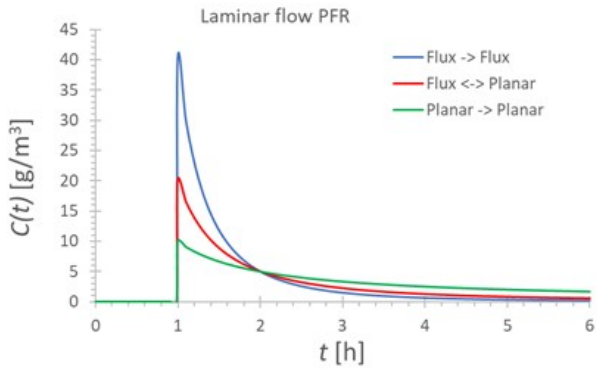

Figure 2.8: *Tracer response curves for laminar flow in pipes. The different output curves change depending on various tracer input and output measurement, retrieved from Kommedal (2022).*

2.3.6 Method of moments analysis

Three parameters are determined from RTD data in the MOM technique (Stephenson & Sheridan, 2021); tracer mass recovery, mean residence time and variance. These represent the zeroth, first and second moment of the tracer response curve.

The zeroth moment is the tracer mass recovery, M_{out}, which can be calculated by the following equation (EPA, 2002; Stephenson & Sheridan, 2021):

$$M_{out} = \int_0^t Q_{out}(t)C_{out}(t)dt = \sum Q_{out}(t)C_{out}(t)\Delta t \tag{2.20}$$

where $Q_{out}(t)$ is the volumetric outflow rate of water at time t, $C_{out}(t)$ is the outlet tracer concentration and Δt is the time difference between measurements. An important requirement for a tracer test to be valid, is that the tracer should be recovered close to its entirety at the outlet. Kadlec and Wallace (2009) refer to tracer recoveries above 80% as acceptable for wetland tracer studies. In addition, the quality of a tracer test can be determined by an accuracy index, A_I (EPA, 2002; Sukhodolov et al., 1997):

$$A_I = \frac{M - \int_0^t Q_{out}(t)C_{out}(t)dt}{M_i} \tag{2.21}$$

where M is the total mass of tracer injected. As A_I approaches 0, the quality of the tracer test increases.

The equations for the first and second moment are reproduced from Tchobanoglous et al. (2014, p. 1933-1935), as described by Levenspiel (1999, p. 262). Normally, the E-curve (RTD) is analysed. In this thesis, however, the C-curve will be applied for the analysis, with equations modified accordingly.

The first moment is the centroid of the tracer response curve and is referred to as the mean residence time, t_m. It describes the average amount of time a fluid particle have spent in the reactor, and is calculated as follows:

$$t_m = \frac{\int_0^\infty tC(t)dt}{\int_0^\infty C(t)dt} \tag{2.22}$$

where $C(t)$ is tracer concentration at time t. From a tracer experiment with defined series of discrete time step measurements, t_m can be approximated to:

$$t_m \approx \frac{\sum t_i C_i \Delta t_i}{\sum C_i \Delta t_i} \tag{2.23}$$

where t_i is time at ith measurement, C_i concentration at ith measurement and Δt_i is the time difference of sample frequency

The second moment, or variance, describes the spread of the tracer as it flows through the reactor, and is given by:

$$\sigma_c^2 = \frac{\int_0^\infty (t-\bar{t})^2 C(t)\,dt}{\int_0^\infty C(t)\,dt} = \frac{\int_0^\infty t^2 C(t)\,dt}{\int_0^\infty C(t)\,dt} - (\bar{t}_c))^2 \tag{2.24}$$

The variance gives an indication of the global mixing in the system (Stephenson & Sheridan, 2021). Experimentally, the variance can be approximated as follows:

$$\sigma_c^2 \approx \frac{\sum t_i^2 C_i \Delta t_i}{\sum C_i \Delta t_i} - (t_m)^2 \tag{2.25}$$

Several tracer studies also include the parameter of effective volume ratio, e, when using the MOM technique. e is described by the ratio between mean residence time and nominal residence time(Bodin et al., 2012; Bodin et al., 2013; Lavrnić et al., 2020; Persson & Wittgren, 2003):

$$e = \frac{t_m}{t_n} = \frac{V_{effective}}{V_{total}} \tag{2.26}$$

where t_n is the theoretical residence time, given by system volume divided by flow rate (V/Q).

Longitudinal Dispersion

The degree of mixing in a system is described by dispersion. As fluid flows through a reactor, some mixing occurs along the flow path. With a tracer test, the rate at which the tracer spreads out along the flow path can be determined from the variance of the tracer curve. Equations 2.27-2.30 are reproduced from Tchobanoglous et al. (2014, p. 1944-1945). A unitless dispersion number can be approximated from the variance and retention time:

$$\frac{\sigma_c^2}{t_n^2} \approx 2d \Rightarrow d \approx \frac{\sigma_c^2}{2t_m^2} \tag{2.27}$$

Tchobanoglous et al. (2014, p. 1945) provide the following list of dispersion numbers and how they relate to degree of axial dispersion in wastewater treatment facilities:

No dispersion	$d = 0$(ideal plug-flow)
Low dispersion	$d = < 0.05$
Moderate dispersion	$d = 0.05$ to 0.25
High dispersion	$d = > 0.25$

For low dispersion, an axial dispersion coefficient is estimated from the unitless dispersion number:

$$d = \frac{D}{\upsilon L} \tag{2.28}$$

where D is the coefficient of axial disperson, L is the characteristic length of the tank and υ is the fluid velocity. For large dispersion, however, axial dispersion is determined from the mean and variance as follows:

$$\frac{\sigma_c^2}{t_m^2} = 2\frac{D}{\upsilon L} + 8\left(\frac{D}{\upsilon L}\right)^2 \tag{2.29}$$

According to Tchobanoglous et al. (2014), the Peclet number of longitudinal dispersion can be further used to characterize the mixing regime from advection and dispersion. If the Peclet number is significantly greater than 1, advection is the primary element of transport. If the number is significantly less than 1 on the other hand, dispersion is considered the primary transport mechanism. For variable flow systems, Persson and Wittgren (2003) points out that the Peclet number is sensitive to changes in water depth. The Peclet number, P_e, is given by the following equation:

$$P_e = \frac{1}{d} \tag{2.30}$$

Shown above, longitudinal dispersion is described by the variance, with related parameters such as the dispersion coefficient and the Peclet number. Various calculation methods of these parameters exist, in addition to those presented here (Persson et al., 1999). Different calculation methods and assumptions make relevant comparisons across tracer studies challenging. In a practical guide for conducting tracer studies in wetlands, a dimensionless variance, σ_θ^2 is presented to represent the mixing conditions (Headley & Kadlec, 2007):

$$\sigma_\theta^2 = \frac{\sigma_c^2}{t_m^2} \tag{2.31}$$

The preceding parameters obtained from the variance, are used to describe mixing, dispersion and velocity profiles. It should be noted that RTD curves (or C-curves) from tracer tests often display a long exceeding tail, with very low concentrations. Such a long tail have a high influence and overestimates the variance. Headley and Kadlec (2007), among others, propose an alternative approach by which the variance is computed from a model of the response curve, in order to minimize the high sensitivity of the long tail. One such model is the TIS-model.

2.3.7 Tank-in-series modelling

Hydraulic behavior of reactors rarely fulfill the flow patterns of an ideal PFR or a CFSTR (Levenspiel, 1999; Tchobanoglous et al., 2014; Werner & Kadlec, 2000). Characterization highly relies on the degree of deviation from these ideal models. One model widely used for modelling hydraulic behavior of wetlands and other reactors is the TIS model (Bodin et al., 2012; Levenspiel, 1999; Stephenson & Sheridan, 2021). When N numbers of equally sized CFSTR tanks are connected in series, the degree of CFSTR and PFR behavior can be described by the number N. If N=1, the reactor behaves like a CFSTR, while N approaching infinity means ideal PFR behavior. The number N can be used to characterize mixing; low N indicates high mixing, while higher N values constitute lower degree of mixing. The TIS-model display a gamma distribution of residence times, and is given by the following equation from Levenspiel (1999, p. 325), modified by Kommedal (2022):

$$C(N,t) = \frac{N \cdot C_0}{(N-1)!} \cdot \left(\frac{t}{\tau}\right)^{N-1} e^{\left(-\frac{N \cdot t}{\tau}\right)} \tag{2.32}$$

where N is the number of reactors, C_0 is pulse-injection concentration, τ is the total retention time for all N reactors. From tracer data, N can be quantified by (with terms specified previously):

$$N = \frac{t_m^2}{\sigma_c^2} \tag{2.33}$$

Persson et al. (1999) use N and e to determine the hydraulic efficiency, λ, which is commonly used to compare designs of constructed wetland:

$$\lambda = e\left(1 - \frac{1}{N}\right) = \frac{t_p}{t_n} \tag{2.34}$$

where t_p is the time of peak, or maximum tracer concentration and t_n is nominal residence time. According to Persson et al. (1999), hydraulic efficiency is classified as poor ($\lambda \leq 0.5$), satisfactory ($0.5 < \lambda \leq 0.75$) and good ($\lambda > 0.75$). One advantage of the λ-parameter is that it avoids the problem of uncertainty related to long residing tails in tracer response curves (Bodin et al., 2012; Persson et al., 1999). Persson et al. (1999) suggest the hydraulic efficiency be used as a parameter to compare shape, inlet/outlet locations and inlet/outlet type for treatment ponds. Although the λ-parameter is commonly used to compare and evaluate treatment performance of constructed wetlands, there is, to the authors knowledge, limited studies on how hydraulic efficiency related to pollution removal by sedimentation. Nevertheless, the determination of hydraulic efficiency of the MSS could still be useful for future studies.

2.3.8 Non-steady state analysis

In the previous sections, the analysis techniques for tracer tests assume steady-state conditions, and the C-curve is used to determine mean residence time, variance with related dispersion and or mixing parameters, and tracer mass recovery. The C-curve is affected by mass of tracer introduced, system volume and flow rate, which makes it challenging to compare with other systems, or the same system under different conditions Headley and Kadlec (2007). Therefore, the curve is normalized to an RTD curve with dimensionless axes. The standard method for normalisation is described by Levenspiel (1999). It is, however, developed for steady-flow systems. Stormwater detention tanks, such as the MSS, are characterized by variable inflow and outflow driven by rainfall events (Raimondi & Becciu, 2017). The variable nature of rainfall causes a continuous process of filling and emptying, and the dynamic flowrates influence the shape of the RTD-curve, which risks a distortion of the actual effect of mixing or dispersion. Analytical methods for RTD analysis of variable flow patterns have been proposed by Werner and Kadlec (1996) and will be presented here.

Principally, the normalising procedure of Werner and Kadlec (1996) removes time from the x-axis. Now, tracer progress on the RTD curve follows the funcion of the proportion of wetland volume flowing through the system. With this volume-based method, tracer studies on both steady and non-steady flow systems can be directly compared.

Varying flow patterns causes the volume of the system to vary over time. Werner and Kadlec (1996) uses tracer mass averaged volume, V_m to determine an average system volume:

$$V_{sys} = V_m = \frac{\int_0^\infty (M_{out} - m_{out}) V_t(t) dt}{\int_0^\infty (M_{out} - m_{out}) dt} \tag{2.35}$$

where M_{out} is the total tracer mass leaving the system, m_{out} is the mass of tracer leaving the system between time increments and $V_t(t)$ is the time average volume:

$$V_t(t) = \frac{\int_0^\infty V(t) dt}{t - 0} \tag{2.36}$$

where $V(t)$ is the system volume at time t. Now, the normalised concentration, $C't$, can be plotted as a function of the dimensionless flow weighted time, ϕ, referred to as the "flow-weighted time RTD function", $C'(\phi)$:

$$C'(\phi) = \frac{C(t) V_{sys}}{M_{out}} \tag{2.37}$$

where ϕ is defined as the ratio of total volume of water exciting the system, V_{out} and V_{sys}:

$$\phi = \frac{V_{out}}{V_{sys}} \tag{2.38}$$

With the normalised RTD function, $C'(\phi)$, the zeroth (M_0^*), the first (M_1^*) and the second (M_2^*) moment of the system can be determined by Equations 2.39-2.41. M_0^* gives the fraction of tracer mass recovered:

$$M_0^* = \int_0^\infty C'(\phi)d\phi \tag{2.39}$$

M_1^* is the centroid of the RTD function:

$$M_1^* = \int_0^\infty \phi C'(\phi)d\phi \tag{2.40}$$

M_2^* represents the variance, ie. the spread of the RTD function:

$$M_2^* = \int_0^\infty (\phi - M_1^*)^2 C'(\phi)d\phi \tag{2.41}$$

Ideal conditions of the normalized RTD function is when M_0^*=1, M_0^*=1 and M_2^*=0. Any deviations are used to characterized the hydraulic efficiency (Werner & Kadlec, 1996).

Theoretically, M_0^*=M_1^*=1 for a normalised RTD with a conservative tracer with no dead zones. For ideal plug flow conditions, M_2^*=0 with no longitudinal mixing. Thus, deviation from the ideal scenario can be used to evaluate the hydraulic behavior of the system (Holland et al., 2004; Werner & Kadlec, 1996).

In an attempt to find an index-value with correlation to pollutant removal, Wahl et al. (2010) proposed the use of a moment index, MI, based on the volume-based RTD analysis with promising results. The MI is derived to avoid reliance on residence time, time-to-peak and variance, which can come short in distinguishing variation. A full elucidation of MI equation will not be given here, but can be found in Wahl et al. (2010). The equation is given as:

$$MI = 1 - \int_0^1 (1 - \phi)C'(\phi)d\phi \tag{2.42}$$

Headley and Kadlec (2007) encourages the adoption of the volume based RTD approach as the standardised method for tracer study analysis, and several studies have answered the call (Aylward et al., 2019; Bodin et al., 2012; Guo et al., 2019; Holcová et al., 2009; Holland et al., 2004).

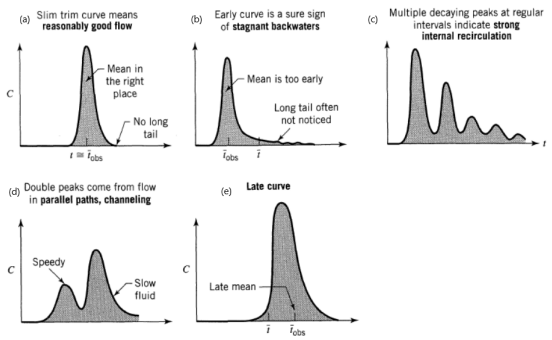

Figure 2.9: *C-curves of misbehaving plug flow reactors from Levenspiel (1999, p. 288), (a) correct mean, (b) mean too early, (c) multiple decaying peak, (d) double peaks and (e) late curve.*

2.3.9 Qualitative tracer curve analysis

The previous section demonstrated the foundation for a quantitative data analysis from a tracer study. A C-curve may also be evaluated qualitatively, as the shape of the C-curve may indicate how the hydraulics diverge from ideal conditions. In Figure 2.9, Levenspiel (1999) illustrates selected C-curves for diagnostic purposes under steady-state flow conditions. The shape of the C-curve depends upon character of the tracer, prevailing flow conditions and the physical design of the hydraulic system (EPA, 2002). With flow conditions in mind, the C-curve show how the shape is affected by faulty flow and Levenspiel (1999) provides suggestions why. Stagnant backwaters is indicated by an early peak, multiple decaying peaks is a sign of strong internal circulation and double peaks may suggest parallel flow paths. If the peak, or mean residence time, is late, Levenspiel (1999) suggest method or assumption errors in the tracer study.

2.3.10 Influence of hydraulic behavior on settling efficiency

The hydraulic conditions within a stormwater treatment reactor can affect the particle removal efficiency. Tchobanoglous et al. (2014) identify eddy currents, thermal convection currents and density current as factors which reduce sedimentation efficiency with respect to TSS removal. These conditions are examples of inadequite mixing, leading to the presence of dead zones, recirculation and parallel fluid channels separated by density properties of the fluid. An example of such conditions are shown in Figure 2.10. Water velocity, and thus the HRT, can be a determining factor in the removal process of

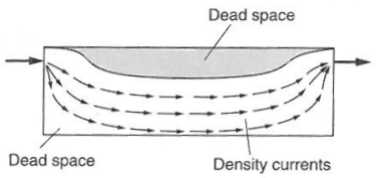

Figure 2.10: *Example of non-ideal flow conditions in a PFR, as illustrated in Tchobanoglous et al. (2014, p. 1932).*

sedimentation, and is highly influenced by short-circuiting and dead-zones (Headley & Kadlec, 2007). Bodin et al. (2012) highlights shape, inlet and outlet location, and inlet design as examples of features that can affect hydraulic behavior, and thus influence settling efficiency in a sedimentation tank. Åstebøl and Hvitved-Jacobsen (2014) also emphasize that the treatment efficiency is connected to not only the HRT, but also mixing at the inlet and if the system has turbulent or laminar flow. Poor design of treatment tanks such as the MSS could result in inadequate mixing and dispersion, which could lead to insufficient treatment with respect to water quality standards. The hydraulic behavior of the MSS will be characterized through a tracer study.

2.4 Rhodamine WT as a tracer in aquatic tracer studies

Rhodamine WT (RWT) is a fluorescent dye commonly used in tracer studies, which is an acknowledged method used to characterize the movements of water and its constituents in both natural and engineered systems. Characteristics of the aquatic system, tracer properties and environmental risks must be considered thoroughly when designing a tracer study. RWT may not always be the best suited tracer. The following review will present an overview tracer study characteristics, physio-chemical properties of RWT, information on toxicity and finally evaluate RWTs suitability for some common aquatic tracer studies. Several tracers have been used successfully in tracer studies, but Tchobanoglous et al. (2014) highlights fluorescein, Rhodamine B and RWT as the most common dye tracers. The following section will further discuss what makes RWT a relevant dye tracer for the planned experiment in this thesis.

2.4.1 Properties Rhodamine WT

RWT is a xanthene dye with fluorescent properties. It has long been a desirable water tracer due to its water solubility, strong fluorescence at low concentrations, low toxicity and low price. It must not be mistaken for Rhodamine B, which is also a fluorescent tracer, but is less water soluble, more toxic and less conservative than RWT (Fernald et al., 2001; Gooseff et al., 2005; Rowiński et al., 2008; Skjolding et al., 2021). The dye is also easily measured in the lab, by hand-held instruments in situ and now also by unmanned airborne vehicles (Johansen et al., 2022). Even without instruments, RWT can be observed with a distinct red/pink color. Figure 2.11 clearly shows the bright pink color of RWT dispersed in the surf zone at Imperial Beach, California (Clark et al., 2014). When exposed to light of the appropriate wavelength, RWT exhibits fluorescence. The excitation and emission wavelengths are 558 nm and 583 nm respectively, as shown in Table 2.2. There has been an increased use of RWT as tracer due to instrumental advances within fluorometry (Baek et al., 2019; Clark et al., 2014; Runkel, 2015; Skjolding et al., 2021). Although tracer studies using RWT may have the purpose of implementing environmental protection measures, RWT could also be a contaminant of environmental risk. Toxicity, environmental quality standards and degradation of RWT must be considered prior to application in tracer studies.

Environmental impact

To evaluate the impact on the environment, some information about bioaccumulation and bio-degradability is useful. A literature search by

Table 2.2: *Physio-chemical properties of RWT (National Center for Biotechnology Information, 2022; Skjolding et al., 2021; Tai & Rathbun, 1988).*

Property	RWT	Unit
Water solubility	18-20	%
Excitation/emission peaks	558/583	λ
logKow	-1.33	
pKa	2.8	
Half life in water summer	15.3	days
Half life in water winter	21.9	days
Photolysis summer	4.77×10^{-2}	per day
Photolysis winter	3.16×10^{-2}	per day

Figure 2.11: *RWT released at Imperial Beach, California. Clark et al. (2014) used RWT to study dispersion and transport in the surfzone near shore.*

Skjolding et al. (2021) did not provide any data on RWTs bioaccumulation or biodegradability. However, as seen in Table 2.2, RWT has a low lipophilicity (logKow < 3), which means it will not readily diffuse across cell membranes to bioaccumulate (National Center for Biotechnology Information, 2022). Skjolding et al. (2021) also reports RWT to be fully ionized at pH > 6, ensuring an even lower lipophilicity at relevant pH values in the environment.

Although there is no available data for the biodegradation, RWT decay by photolysis, and rate coefficients were found at a range from 4.77×10^{-2} per day for summer and 3.16×10^{-2} per day during winter (Tai & Rathbun, 1988). Up until recently, ecotoxicological data for RWT has been limited. Some studies have tried to address its environmental safety (Behrens et al., 2001; Field et al., 1995; Parker Jr, 1973; Rowiński & Chrzanowski, 2011), but these studies do not meet the requirements to present regulatory measures. In order to qualify as regulatory threshold limits, such as Environmental Quality Standards (EQS), standardized ecotoxicity tests must be performed (EC, 2018). Skjolding et al. (2021) thus applied a series of short-term standardized toxicity tests across the needed range of trophic levels and were able to determine limit values of RWT to ensure the protection of aquatic species against effects. These toxicity tests resulted in a PNEC of 91 μg/L which was used to estimate EQS values of annual-average quality standard (AA-QS) and maximum allowable concentration quality standard (MAC-QS), respectively

Table 2.3: *Predicted no effect concentration (PNEC) and estimated environmental quality standards (EQS) of RWT (National Center for Biotechnology Information, 2022; Skjolding et al., 2021).*

Environmental quality standards	Value	Unit
$PNEC_{aq}$	91	μg/L
AA-QS	91	μg/L
MAC-QS	910	μg/L

>91 μg/L AA-QS and >910 μg/L MAC-QS as reported in Table 2.2. MAC-QS is highly relevant for tracer studies, as this represents short, intermittent exposures with duration lower than 24 h.

An appropriate design of a tracer study using RWT can now apply established toxicity threshold limits and environmental quality standards. However, several studies have shown that RWT present some challenges related to sorption.

Sorption limitations

According to a review study by Runkel (2015), RWT has traditionally been considered nominally conservative. As early as 1968, Wilson et al. (1986) stated RWT was "reasonably stable" with "low sorptive tencency". The same work did, however, indicate that sorption of RWT would be a critical factor for groundwater tracer studies. In fact, several ground water studies have applied RWT as a surrogate for organic contaminants due to its sorption behavior. (Everts & Kanwar, 1994; Sabatini & Austin, 1991). The following paragraphs will give a brief summary of the findings of Runkel (2015), which suggest RWT display a differing grade of conservative behavior depending on the system to be studied.

When considering the adsorption properties of RWT, it is necessary to distinguish between which hydraulic processes the tracer study is meant to describe. Runkel (2015) describe three different applications of tracer studies:

i. Traveltime studies: To quantify time of travel in rivers, streams, wetlands or other engineered reactors in order to estimate parameters such as residence time of the water in the system (Fall et al., 2012; Keefe et al., 2004; Rivord et al., 2014)

ii. Hyporheic zone and transient storage studies: To quantify and characterize how water by the streambed interacts with overlying surface water (Gooseff et al., 2005).

iii. Groundwater systems: RWT is used as a tracer to mimic the sorption of organic contaminants in the groundwater (Mukherjee et al., 2005)

Some of these hydraulic processes are more affected by adsorption of RWT than others. Several studies have documented adsorption of RWT by checking the mass recovery (Lin et al., 2003; Ruehl et al., 2006; Writer et al., 2012). The loss of RWT mass during these experiments is mainly attributed to adsorption. Photochemical decay, as indicated in Table 2.2, have minimal consequence during the time scale of the experiments (Lin et al., 2003; Smart & Laidlaw, 1977). Coinjection studies have compared results achieved by using both RWT and bromide as tracers reporting a lower mass recovery by RWT than bromide (Cox et al., 2003; Dierberg & DeBusk, 2005; Lin et al., 2003; Ruehl et al., 2006). Despite lower mass recovery of RWT, Runkel (2015) points out that the tracer response curve showed close correspondence with bromide, which allowed for precise estimation of residence time in traveltime studies. The same correspondence did not hold true for tracer curves in coinjection studies for quantifying the hyporheic zone. Bencala et al. (1983) found the RWT concentration peak to be 55% lower than expected from a chloride tracer, and Mukherjee et al. (2005) also had "dramatically different" estimations from RWT and bromide for storage zone transport in streams.

Adsorption influences the results of hyporheic zone studies significantly because RWT has increased contact with sediments. Runkel (2015) suggest the storage zones of water mass by the streambed has more time to interact with solid surfaces making it more affected by sorption. Traveltime studies on the other hand, mostly relies on tracer mass transported by the advective channel and the large volume of water to surface area ratio limits adsorption of RWT to sediments. To illustrate, Runkel (2015) uses the tracer response curve, as described in the previous section, to explain that the hydraulic parameters of a traveltime study is depicted from the bulk of tracer mass represented by the part of the curve preceding the tail, while hyporheic zone studies rely on the tracer mass in the tail of the tracer curve.

Several studies report an increase in RWT sorption with increased organic matter content (Dierberg & DeBusk, 2005; Lin et al., 2003; Smart & Laidlaw, 1977). It does not, however, justify the assumption of conservative behavior of RWT in systems with minimal presence of organic matter (Runkel, 2015). RWT can also adsorb onto inorganic sediments and materials such as silica, sand and metal oxides (Bencala et al., 1983; Kasnavia et al., 1999; Shiau et al., 1993).

The preceding paragraphs have shed some light on how RWT may be considered both conservative and non-conservative depending on hydraulic system to be studied. Runkel (2015) distinguishes particularly between

traveltime studies for estimating residence time and characterizing physical parameters of hyporheic zone processes. Conservative behavior of RWT may be assumed for traveltime studies, but not for hyporheic zone processes. Runkel (2015) provide an example of proper use of RWT; to estimate the HRT for the purpose of nutrient uptake in constructed wetlands. Such an example is highly comparable to the process in the MSS, where residence time is an essential design parameter for the settling of particles.

2.4.2 Rhodamine WT as tracer for sedimentation tank analysis

RWT is clearly a popular dye tracer for aquatic tracer studies for several reasons. The tracer is considered cheap and its fluorescent properties allows for acceptable concentration detection even at low concentrations. Recent improvement in instrumental measuring technologies for fluorescence in situ has increased the interest for RWT. Factors related to environmental risk and adsorption have to be considered before moving forward with RWT as a tracer in a stormwater sedimentation facility. Threshold limits for EQS are estimated to 91 μg/L (AA-QS) and 910 μg/L (MAC-QS) (Skjolding et al., 2021). Thus, concentrations less than 910 mug/L of RWT will not pose a risk to aquatic life during the proposed tracer experiment. Adsorption of RWT is influenced by type of aquatic system to be studied, mainly depending on how close and for how long the tracer interacts with solids such as sediments in the stream. Runkel (2015) concludes sorption will minimally affect the estimation of hydraulic parameters such as residence time. The tracer study for the stormwater sedimentation facility involves a traveltime study with the main purpose of estimating residence time. In light of the preceding discussion, RWT is a justified choice of tracer for our study.

2.4.3 Fluorescence: Instrumental analysis of RWT

In situ monitoring of RWT during the tracer study will be performed with a fluorometry sensor. Understanding what fluorescence is, how the technology works and its limitations is essential for ensuring precise methodology and data analysis.

The EXO Total Algae Phycocyanin Smart Sensor (TAL-PC) is designed to detect fluorescence in the algae pigments of phycocyanin (PC) (YSI, 2020). Fluorescence is explained by excitation and emission of energy. When a fluorescent substance, such as RWT or PC is exposed to a light source of a particular wavelength, electrons are excited which puts the substance in a

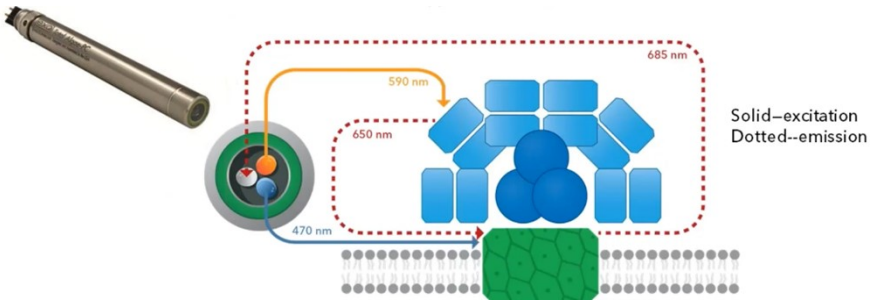

Figure 2.12: *Fluorescence principle of the TAL-PC sensor. Retrieved from YSI webinar series (Smith, 2019).*

higher energy state. When the electrons return to normal position, energy in the form of light is emitted (fluoresced). Each fluorescent molecule has a specific excitation and emission spectra, a principle utilized in instruments for analysing fluorescence (Wilson et al., 1986). The TAL-PC sensor uses orange LED light to excite electrons at wavelength 590 ± 15 nm, and the sensor is set to detect emission wavelengths of 685 ± 20 nm (YSI, 2020), as illustrated by Smith (2019) in Figure 2.12.
Although the sensor is developed for the pigment PC, it can still detect fluorescence of RWT as the excitation and emission spectra of RWT overlaps with sensor detection range (Smith, 2018).

Measurement errors

Tracer concentration measurements consists of two parts; true tracer concentration, C_Υ, and measurement error concentration, C_ϵ, as described by the following equation (Field, 2020):

$$C = \sum_{i=1}^{n} C_{\Upsilon_i} + C_{\epsilon_i} \tag{2.43}$$

Measurement errors can be separated into two groups: systematic errors associated with the analytical instrument, and random errors which are a result of factors which cannot be predicted. Random errors can be revealed by repeated measurements. Systematic errors can be related to instrumental drift, miscalibration and sensor fouling. These errors are inflicted on all measurements, in the same way and to the same extent and cannot be revealed by repeated measurements (Field, 2020; Taylor, 1997). Instrument calibration and validation according to standards is essential to minimize systematic errors (EPA, 2002, 2017; Wilson et al., 1986). For a large-scale tracer study, the variable and unpredictable nature of rainfall events, and

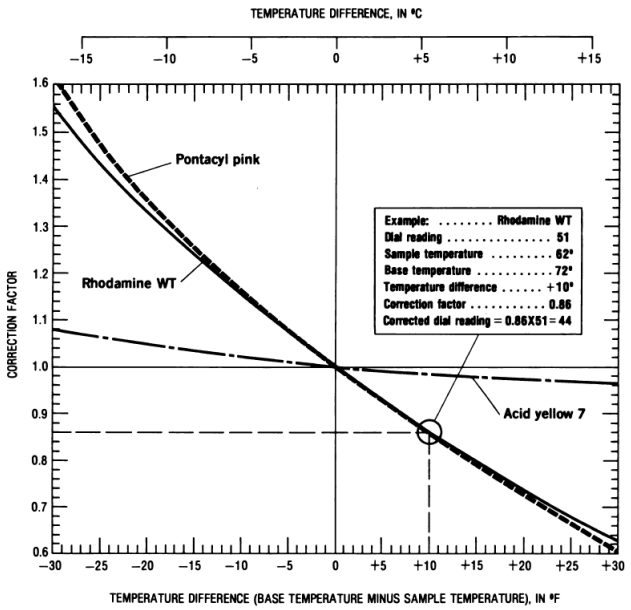

Figure 2.13: *Temperature-correction curves for RWT and other tracer dyes, as seen in Wilson et al. (1986).*

practical limitations of acquiring enough water, repeated measurements are considered unrealizable. A statistical analysis will thus not be possible for a tracer study of the MSS.

There are, however, other sources of error which adversely affect precise concentration measurements: Temperature effect and background tracer concentrations (EPA, 2002; Field, 2020). Wilson et al. (1986) states that temperature is the most significant factor which influences fluorescence. Higher temperatures increase fluorescent activity which can give higher readings. Temperature effects can be accounted for in data analysis by using the temperature-correction curve for RWT, presented by Wilson et al. (1986) in Figure 2.13.

Water samples could contain some background fluorescence which must be subtracted from measured fluorescence. Before tracer injection, background fluorescence should be monitored and analyzed. Ideally, background levels should be recorded in advance, during and after the tracer experiment. Background monitoring during the tracer study is problematic as the tracer signal occurs on top of the background and obscures the measurements. Field (2020) mentions spectral deconvolution as a potential solution to this problem, but this is beyond the scope of this thesis. To simplify calculations, a selected number of background measurements are collected and averaged prior to tracer release. If low enough (a few μg/L),

the final average background concentration, $\overline{C}_B$, is subtracted from each tracer measurement, C_i, during the experiment, as described below (EPA, 2002; Field, 2020; Wilson et al., 1986):

$$C = \sum_{i=1}^{n} C_i - \overline{C}_B \tag{2.44}$$

where C is considered the true concentration for further analysis, and

$$\overline{C}_B = \frac{1}{n} \sum_{i=1}^{n} C_{B_i} \tag{2.45}$$

Summarized, three steps are essential when taking fluorescence measurements to minimize measurement errors: (1) proper instrument calibration, (2) temperature correction for temperature difference between calibration water and sample water and (3) background fluorescence correction.

2.5 Thesis Objective

Stormwater detention tanks are designed primarily for flood protection, whereby calculations are done to estimate the required detention volume of increased stormwater load. These tanks also have the potential for pollution protection through sedimentation of particles. With increased urbanization and global warming, such facilities are essential in stormwater management. Design guidelines for detention tanks are well established with respect to water detention. However, clear design guidelines with respect to treatment efficiency are lacking. The MSS has been designed for the dual-purpose of detention and particle sedimentation. Previous studies have thoroughly tested the MSS for performance in terms of pollutant removal under various precipitation events (Bergseng, 2021; Gausel Lode, 2021). These studies give information about the removal efficiency of the MSS, but they provide limited data on how such a system could be optimized by design to improve the removal efficiency. Hydraulic retention time, mixing and flow regime should be characterized to determine the adequacy of reactor design to identify potential reactor problems. Normally, the HRT is a determining factor for treatment efficiency for sedimentation, and can be calculated simply during steady-flow conditions of constant volume and flow. To the authors knowledge, there are limited studies on hydraulic behavior of stormwater detention tanks with conditions of variable flow. This is not the case in the field of constructed wetlands, however, whereby methods have

been adapted to analyse and compare wetlands of with different design configurations and operational conditions of variable flow.

This thesis will use a tracer study to characterize the hydraulic behavior of the MSS, as a step to identify factors for future design improvements. Tracer study data will be analysed according to methods based on the assumption of steady-flow conditions, in addition to presented methods for variable flow. The application of different methods will be used to clarify which methods are more appropriate for sound tracer data analysis of stormwater detention tanks.

3. Methods

This section presents a description of study site, instrument calibration, water sampling in the field and the method for tracer curve analysis.

3.1 Site description

The underground modular settling tank, MSS, to be studied is located by the regional highway Fv 505, in Sandnes, Norway. Stormwater from a catchment of 1.44 ha, involving a four-lane road surface with a bridge and roundabout, runs through three parallel settling tanks, each with a diameter of 2400 m and length of 27.7 m. Combined, the system has a detention volume of 154 m^3 (Storm Aqua AS, 2021). A technical drawing of the facility can be seen in Figure 3.1. Particle bound pollutants are removed through sedimentation according to NPRA's design handbook N200 (NPRA, 2018). Larger particles and floatables are removed prior to the settling tanks in a 2500 mm manhole. After treatment, the water from all three tanks are led into the same gully pot. The water then flows through pipes into the river, Figgjovassdraget. A more detailed system description can be found in Storm Aqua AS (2021).

The detention of water in the settling tank is controlled by a 50 mm outlet pipe. As the outlet pipe in the discharge control manhole is smaller than the inlet pipe (250mm), detention is achieved and observed by the rising water level in the sedimentation tank. If the tank is completely filled with water, the system will go into overflow and water will spill over a wall in the discharge control manhole. The water level in the settling tank (2400 mm) is at a minimum of 1350 mm, which is the outlet height.

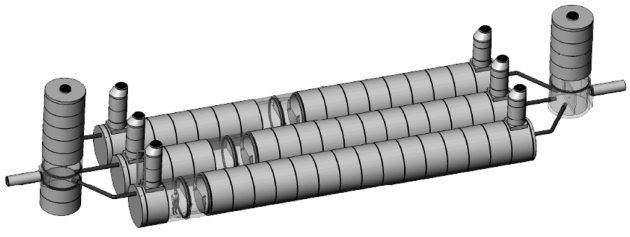

Figure 3.1: *Technical drawing from Storm Aqua AS (2021).*

3.2 Materials

An overview of instruments and chemicals used is presented in this section, along with instrument calibration and validation procedure.

3.2.1 Chemicals

RWT was used as tracer dye based on the evaluations made in section 2.4. For the calibration curve, a strong working standard (10 000 μg/L) and a weak working standard (100 μg/L) of RWT in distilled water were prepared using RWT 20 % (w/v, Thermo Fisher Scientific, VWR: cat. no 446970010). These were further diluted to make nine calibration solutions (see section 3.2.3. For the tracer experiments, 200 mL of the RWT 20% was used directly for influent injection.

3.2.2 Analytical instrument

Tracer dye concentration was monitored by a YSI EXO1 sonde (YSI,Inc.), installed by the outlet pipe of the settling tank. The YSI sonde was equipped with an fluorescence sensor, a TAL-PC sensor and a temperature probe resolving to $\pm$0.01°C. The sensor was calibrated for RWT concentration as described in Section 3.2.3. In addition, capable of resolving depth to $\pm$4 mm, the YSI sonde monitored tank volume based on depth measurements.

3.2.3 Flowmeter

Two flowmeters (2150 Area Velocity Module, Teledyne ISCO)) were already installed by the Norwegian Institute for Water (NIVA) at the MSS. One was installed by the inlet, in a pipe leading into the first 2500 mm manhole, while the other was installed by the final outlet, after the discharge control chamber. Both monitored volumetric flow rate every 5 min.

Calibration

The TAL-PC sensor came with a manufacturer's calibration method for RWT with the purpose of correlating RWT with phycocyanin in algae, which was not relevant for the purpose of this study. Calibration was performed according to Operating Procedure (OP) for Dye Tracer Measurements (EPA, 2017), with a series of nine RWT standard solutions, and was adapted with certain recommendations from "Fluorometric Procedures for Dye Tracing" (Wilson et al., 1986).

In order to avoid RWT absorption by rubber and polyethylene, glassware equipment was used where possible as recommended by Wilson et al. (1986). RWT standard solutions were prepared volumetrically by diluting RWT 20 % with distilled water. Pipetting was performed with Finnpipette F2 Variable volume pipettes (Finntip 5mL, Thermo Scientific) and glassware 25 mL bulb pipettes. Solutions were mixed with distilled water in glassware volumetric flasks of 500 mL or 1000 mL. Each solution was transferred into a calibration cup provided by the manufacturer for analysis with the TAL-PC sensor. Tap water was used for the calibration blank. A complete overview of dilution volumes and concentrations can be found in Appendix B, along with a more detailed procedure description.

Each sample was immersed for one minute. Readings of PC-RFU, relative fluorescence units, were recorded and plotted for a calibration curve in Excel. The Excel linear regression analysis function was used to determine a linear regression line, uncertainty, and limit of detection. The level of confidence was set to 95%.

RWT concentrations were calculated using the linear regression with the formula:

$$C_{RWT} = \frac{y - b}{a} \tag{3.1}$$

where a is the slope of the calibration curve, b is the y-intercept and y is the RFU reading from the TAL-PC sensor.

The sensitivity, or limit of detection (LOD) of the TAL-PC sensor was found using the following equation (Center for Biologics Evaluation and Research, 2021).

$$LOD = \frac{3.3\sigma}{a} \tag{3.2}$$

where σ is the residual standard deviation from the linear regression analysis and a is the slope of the calibration curve.

Error propagation from calibration curve

For a measured concentration of C_{RWT}, s_C is the uncertainty (reported as $C_{RWT} \pm s_C$), derived from the error propagation of the calibration line (Taylor, 1997):

$$\frac{\delta C}{\delta a} = -\frac{1}{1}\frac{y - b}{a^2} \tag{3.3}$$

$$\frac{\delta C}{\delta b} = -\frac{1}{a} \tag{3.4}$$

$$s_C = \sqrt{\left(\frac{\delta C}{\delta a} a\right)^2 + \left(\frac{\delta C}{\delta b} b\right)^2} \tag{3.5}$$

Validation of calibration curve

As specified by the OP (EPA, 2017), the calibration was followed by a verification procedure. Two randomly chosen RWT solutions with known concentrations of 200 μg/L and 800 μg/L were prepared for RFU measurement in the calibration cup. The two solutions were also mixed for a third validation solution of 500 μg/L. Concentrations were then calculated using the above equation, and checked towards the known concentrations, in order to verify if the instrument readings were within $\pm$10 % of the calibration standards (EPA, 2017).

The linear regression analysis, limit of detection and results from the validation analysis can be found in section 4.

3.3 Tracer study setup

Two tracer experiments were set up at the site in November and December 2022. Experiment 1 was performed during dry weather conditions, with a pump providing constant inlet flow. Experiment 2 was done with rainfall events providing varying inlet flow. Each experiment, tracer injection and tracer sampling is described more detailed in the following sections.

3.3.1 Experiment 1

In order to minimize flow variables, experiment 1 was performed during dry weather conditions, over the course of two days: November 14-15, 2022. Settling tank 1 was selected as the tracer study reactor. A pump was installed to pump water directly from settling tank 3, into the inlet of settling tank 1. As soon as settling tank 3 was empty, the pump was moved to settling tank 2. Time of pump transfer was recorded to 14 min. Inlet flow was measured manually before injection of tracer, and directly after pump transfer. The inlet flow was measured manually with a stopwatch and a 250 L oil drum. The inlet flowmeter was installed prior to the inlet of the pump, which excluded the use of the inlet flowmeter. Pumping was stopped when settling tank 2 was empty, while the tracer sampling continued until the water level stabilized below the

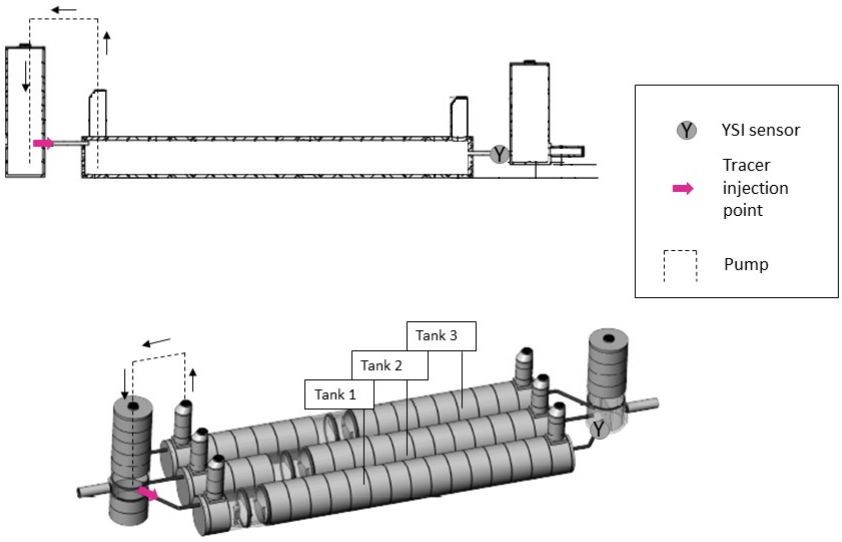

Figure 3.2: *Schematics of the tracer study setup at the MSS at Fv505, Sandnes. The pump was used for experiment 1, but not experiment 2. Position of tracer injection point and YSI sensor remain the same for both experiments. Modified from Storm Aqua AS (2021).*

outlet and outflow stopped. Limited water access, cost, and minimal dry weather conditions, excluded the possibility of replication.

3.3.2 Experiment 2

Experiment 2 was performed with rainfall events during December 20-22, 2022. Settling tank 1 was selected as the tracer study reactor, while tank 2 and 3 were closed by the inlet, in order to ensure enough inlet water to obtain a complete tracer output curve. Inlet flow for the tracer study was driven by rainfall events, and inflow rate was measured by the inlet flowmeter. Tracer injection and sampling was performed as described in respective sections below. This experiment relied on multiple precipitation events to complete the tracer output curve, and due to the unpredictable time frame, replication was not possible.

3.3.3 Tracer injection

Mass of RWT injection was determined by the following considerations: (1) RWT concentration in the mixing zone could not exceed the MAC-QS of 910μg/L, in order to avoid potential environmental risk in receiving streams, (2) RWT concentrations should be sufficiently above analytical detection limits.

In both experiments, 200 mL of RWT 20% was pulse-injected (within 4 min) by submerging a graduated cylinder with the RWT solution into the inlet pipe for settling tank 1. The graduated cylinder was submerged and rinsed with inlet water several times to ensure complete solution injection. Time of tracer injection was considered short compared to theoretical residence time of the system, which allowed for the assumption of negligible dispersion between injection point and system feed.

3.3.4 Water samples

The dye was monitored *in situ* in the outlet pipe by use of the YSI sonde, equipped with the TAL-PC sensor. The sonde was mounted into a fixed, horizontal position in the outlet pipe of settling tank 1, as illustrated in Figure 3.3 and 3.4. Pictures of the setup can be found in Appendix C. A connected datalogger (EXO Handheld Display, YSI, Inc.), logged fluorescence readings every two minutes.

The outlet flowmeter recorded effluent flow every five minutes. Tracer monitoring concluded when fluorescence readings reached background levels. For Experiment 1, the tracer experiment concluded when the water level stabilized and no flow was going through the reactor.

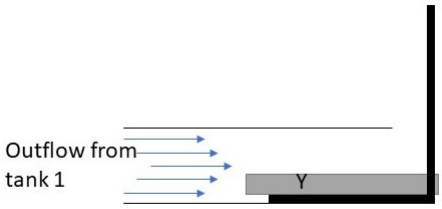

Figure 3.3: *Schematic illustration of EXO1 sonde mounted in outlet pipe from settling tank 1.*

Figure 3.4: *YSI sonde secured to steel bar.*

Measurement errors

Tracer concentration measurements are affected by systemic errors and random errors. Systemic errors were minimized by calibration and validation, as described earlier in this chapter. Due to practical limitations, random errors could not be accounted for by repeated measurements. Nevertheless, the effect of temperature and background concentration were minimized as described in the following section.

Correction for background and temperature

All fluorescent measurements were corrected for background measurements after calibration of the instrument. Prior to tracer injection, background fluorescence was recorded and averaged. The average background fluorescence was subtracted from the fluorescence measurements during the tracer study.

Temperature correction factors were determined by the use of Figure 2.13 in section 2.4.2. Fluorescence measurements for continued used in the tracer analysis were then given by

$$RFU_i = T_{cf} \times (RFU_m - \overline{RFU}_B) \tag{3.6}$$

where T_{cf} is temperature correction factor, RFU_i is corrected fluorescence measurement, RFU_m is fluorescence measurement and $\overline{RFU}_B$ is average background fluorescence measurement.

3.3.5 Estimation of flow and volume

The MSS had a flowmeter installed by the final outlet after the discharge control chamber which monitored discharge every five minutes. During both experiments, the outlet flowmeter showed inconsistent behavior with spiked noise during overflow conditions (i.e outliers). Some recordings were also blank during the experiment, which limited the quality of data from the flowmeter.

An alternative approach for discharge determination was proposed through the principle of energy conservation, derived from Bernoulli's equation: Outflow, Q_{out} was calculated according to the Torricelli formula for flow through an orifice. This method is also suggested for flow estimation in the design document for the MSS (Ødegaard, 2014; Storm Aqua AS, 2021):

$$Q_{out} = cA\sqrt{2gH} \tag{3.7}$$

where c is the orifice coefficient (0.36), A is the orifice(outlet pipe) cross-sectional area (pipe diameter=50 mm), g is the gravity acceleration and H is the height of liquid above the middle of the orifice. The recorded depth from the YSI-sonde was used to calculate tank volume and flow at each time increment. Inflow (Q_{in}), and outflow (Q_{out}) rates were used to estimate the Q_{mean} for determination of the nominal residence time (Lavrnić et al., 2020):

$$Q_{mean} = \frac{Q_{in} + \overline{Q}_o ut}{1} \tag{3.8}$$

where $\overline{Q}_{out}$ is the mean outflow rate from outflow estimations.

For Experiment 1, calculation of sedimentation tank volume was based on water depth measurements. As the depth measurements were not calibrated for true volume, a baseline was set according to max water depth when the system was in overflow. During overflow, the MSS was full, and the water depth was adjusted to the known diameter of the tank, 2.4 meters, and the offset was used to all water level measurements.

In Experiment 2, depth measurements were adjusted according to the offset found from the lowest water level with corresponding minimal system inflow, with the assumption the water level was below the height of the outlet (H=1.35 m). These data were further used to estimate outflow rate by Torricelli's formula, as described for Experiment 2.

Volume was determined with the formula for partially filled horizontal cylinders with terms shown in Figure 3.5:

$$V = L\left(R^2 cos^{-1}\left(\frac{R-D}{D}\right) - (R-D)\sqrt{2RD - D^2}\right) \tag{3.9}$$

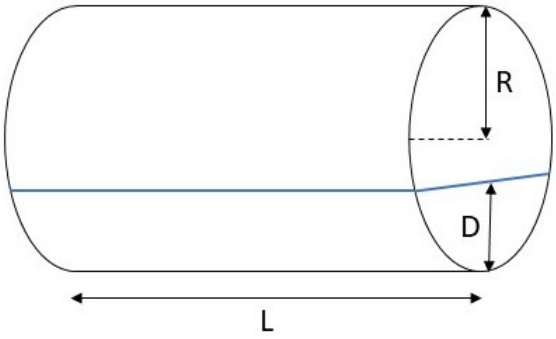

Figure 3.5: *Terms for a partially filled, horizontal cylinder.*

where L is the length of the tank (27.7 m), D is the water depth inside the tank and R is the radius of the tank (1.2m).

The depth and flow curve was plotted versus time.

3.4 Data analysis

The shape of produced C-curves were compared to PFR C-curves from Levenspiel (1999) as shown in Figure 2.9, for a qualitative analysis. Then, the tracer data from Experiment 1 was analysed with the different techniques described in section 2.3; MOM-analysis, volume-based RTD analysis for non-steady flow, the LCF-model and the TIS-model. Data analysis of Experiment 2 only involved the volume-based RTD analysis. The nominal retention time ($t_n = V/Q$) and Reynolds number (N_R) were estimated by using the average V_{sys}, and Q_{mean} from flow estimations. The hydraulic characterisation parameters were used to describe the flow regime, hydraulic retention time, mixing and short-circuiting and were further evaluated towards effect on sedimentation.

3.4.1 Method of moments

Tracer sampling data was used to plot a C-curve. Tracer test quality was evaluated based upon tracer mass recovery and the accuracy index. Hydraulic characterisation of mean residence time (t_m), variance (σ_c^2), dispersion coefficient (D) and the Peclet number was done with equations listed in Section 2.3.6. Where necessary, fluid velocity, ($\upsilon = Q/A$), was

calculated from Q_{mean} and cross-sectional area of V_{sys}. Equations for MOM-analysis are summarized in Table 3.1.

3.4.2 Volume-based RTD

The C-curve was normalised according to the volume-based RTD approach, and the new dimensionless RTD, $C'(\phi)$, was plotted versus flow weighted time, ϕ. Furthermore, the zeroth, first and second moment, along with the dimensionless variance was calculated as summarized from the bottom in Table 3.1. Background for calculations are found in Section 2.3.8.

3.4.3 Models and curve fitting

Both the LCF-model and TIS-model was produced by using the sum of squared errors (SSQE) to find the best fit to the tracer response curve. The SSQE minimized the difference between model concentration($C_m(T)$) and measured concentration ($C(t)$ of tracer:

$$SSQE = \sum (C(t) - C_m(t))^2 \tag{3.10}$$

Input hydraulic parameters for the models were estimated with The Solver application in Microsoft Excel. The Solver was set to minimize the $SSQE$ by changing the model input values of mean residence time (t_m) for the laminar convection model, and also the number of tank in series, N, for the TIS-model. N and λ was also determined from tracer data. The model functions and equations for hydraulic parameters are summarised in Table 3.2.

3.4.4 Sedimentation analysis

Equation 2.5-2.11 were used to calculate the minimum particle settling velocity for TSS larger than 0.45μm. Settling velocities and average water depths (from V_{sys}) were used to calculate time needed for sedimentation (Equation 2.12), which were further compared to the hydraulic retention time from the tracer studies.

Statistical analysis was not performed for this study due to the practical limitations of the variable nature and unpredictability of rain events necessary for tracer studies.

3.4.5 Statistical analysis

Due to practical and economic limitations, replications of tracer studies were not possible. As a result, no statistical analysis was performed.

Table 3.1: *Equations for reactor analysis with method of moments technique and the volume-based RTD approach.*

Hydraulic parameter	**Equation**	**Eq no.**
Tracer mass recovery, MR	$MR = \frac{\int_0^t Q_{out}(t)C_{out}(t)dt}{M}$	2.20
Accuracy index, A_I	$A_I = \frac{M - \int_0^t Q_{out}(t)C_{out}(t)dt}{M}$	2.21
Mean residence time, t_m	$t_m = \frac{\sum t_i C_i \Delta t_i}{\sum C_i \Delta t_i}$	2.23
Nominal residence time, t_n	$t_n = \frac{V_{sys}}{Q_{mean}}$	
Effective volume ratio, e	$e = \frac{t_m}{t_n}$	2.26
Variance, σ_c^2	$\sigma_c^2 \approx \frac{\sum t_i^2 C_i \Delta t_i}{\sum C_i \Delta t_i} - (t_m)^2$	2.25
Unitless variance, σ_θ^2	$\sigma_\theta^2 = \frac{\sigma^2}{t_m^2}$	2.31
Unitless disperison, d	$d \approx \frac{\sigma_c^2}{2t_m^2}$	2.27
Coefficient of dispersion (low), D	$d = \frac{D}{vL}$	2.28
Coefficient of dispersion (mod), D	$\frac{\sigma_c^2}{t_m^2} = 2\frac{D}{vL} + 8\left(\frac{D}{vL}\right)^2$	2.29
Peclet number 1, P_{e_1}	$P_{e_1} = \frac{1}{d}$	2.30
Hydraulic Efficiency, λ	$\lambda = e\left(1 - \frac{1}{N}\right) = \frac{t_p}{t_n}$	2.34
Flow-weighted time	$\phi = \frac{V_{out}}{V_{sys}}$	2.38
Zeroth moment	$M_0^* = \int_0^\infty C'(\phi)d\phi$	2.39
First moment	$M_1^* = \int_0^\infty \phi C'(\phi)d\phi$	2.40
Second moment	$M_2^* = \int_0^\infty (\phi - M_1^*)^2 C'(\phi)d\phi$	2.41
Moment index	$MI = 1 - \int_0^1 (1-\phi)C'(\phi)d\phi$	2.42

Table 3.2: *Functions and equations used for LCF and TIS-modelling.*

Model/parameter	**Function/equation**	**Eq no.**
LCF-model $Flux \rightarrow Flux$	$C(t)_{F,F} = \frac{M_0}{V} \cdot \frac{\overline{\tau}^3}{2t^3}$	2.17
LCF-model $Flux \leftrightarrow Planar$	$C(t)_{F,P} = \frac{M_0}{V} \cdot \frac{\overline{\tau}^2}{2t^2}$	2.18
LCF-model $Planar \rightarrow Planar$	$C(t)_{P,P} = \frac{M_0}{V} \cdot \frac{\overline{\tau}}{2t}$	2.19
TIS-model	$C(N,t) = \frac{N \cdot C_0}{(N-1)!} \cdot \left(\frac{t}{\tau}\right)^{N-1} e^{\left(-\frac{N \cdot t}{\tau}\right)}$	2.32
Number of tanks in series	$N = \frac{t_m^2}{\sigma^2}$	2.33
Hydraulic efficiency	$\lambda = e\left(1 - \frac{1}{N}\right) = \frac{t_p}{t_n}$	2.34

4. Results and discussion

In this chapter, the results of the tracer study are presented and discussed. First, the results from the methodological evaluation are described, followed by the results and analysis of the tracer study. Section 4.8 gives an overview of limitations in this project, and finally Section 4.9 provides suggestions for future work.

4.1 Methodological evaluation

A description of background and temperature corrections, a calibration regression analysis and validation test results are presented here.

4.1.1 Regression analysis and limit of detection

The calibration curve for RWT fluorescence is shown in Figure 4.1. The coefficient of determination, R^2, was calculated to be 0.999, which shows a strong linear relationship between measured fluorescence and RWT concentration. The regression line is represented by a slope and y-intercept, and their uncertainties are listed in Table 4.1.

One purpose of the calibration curve is to determine the linear range of the TAL-PC sensor. Instrument specifications list a linear accuracy between 0-100 RFU (YSI, 2020) and with a RFU reading of 145.57 RFU, solution D1 is outside the specified range. In addition, a linear regression of results including D1 showed a y-intercept of 2.34, which could indicate quenching, whereby the fluorescence intensity of the high concentration D1 decreases. According to Wilson et al. (1986), fluorescence varies linearly with concentration, except at very high concentrations above several hundred micrograms per liter, and quenching can be observed at such high concentrations. The decision to omit D1 of 10 000 μg/L can thus be justified considering the RFU reading outside

Table 4.1: *Regression analysis of calibration curve.*

Regression line variables	**Value**	**Standard deviation**	**Uncertainty (95 % conf. interval)**
Slope	0.0288	0.0002	± 0.0005
Y-intercept	0.0787	0.0823	±0.1946

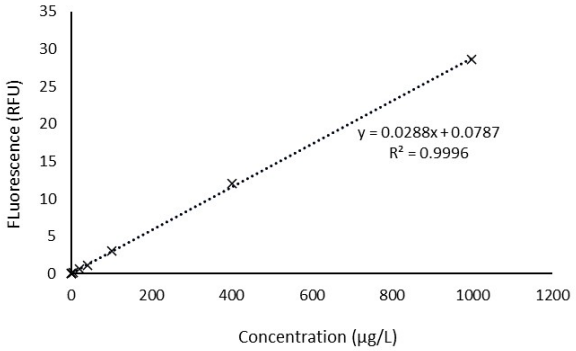

Figure 4.1: *Calibration curve with fluorescence, RFU, plotted against standard concentrations of Rhodamine WT, µg/L.*

the instruments specified linear range, and the warnings of quenching from Wilson et al. (1986).

The error analysis estimated the standard deviation of the response to be 0.2164, which gives an instrument sensitivity of 24.8 μg/L. According to this regression analysis of the calibration curve, the TAL-PC sensor will not show reliable fluorescence intensities for RWT concentrations below 24.8 μg/L. In an attempt to evaluate TAL-PC sensors performance on measuring Rhodamine WT in a stream, the sensor manufacturers (YSI) found that "when Rhodamine concentrations dipped into the 20s (μg/L), readings get a little rockier", and suggested the sensor showed noise at such low ranges (Smith, 2021). Although D9 was outside the linear range, an upper limit was not investigated. YSI (2020) specifies 100 RFU as an upper limit. This could be looked into by extrapolating from the regression line but was found to be unnecessary in this study. The planned tracer analysis will not use concentrations which can produce a fluorescence intensity that high. The maximum allowable toxicity limit of 910 μg/L RWT is within the range covered by the calibration standards.

4.1.2 Validation of calibration curve

The validation results are presented in Table 4.2, where the measured concentration is calculated from the regression line. All validation solutions were measured to a lower concentration than what was prepared. V1 and V2 were prepared separately from the RWT 20% solution, and the higher percentage of difference for V1 of 7.6% indicates random error in the volumetric dilution method of V1. The mixed solution, V_{1+2}, shows a similar difference percentage as for V1, which confirms a carryover of random error

Table 4.2: *Validation results.*

Solution	**Measured concentration** [1]	**Prepared concentration** [2]	**Difference measured and prepared**
	μg/L	**μg/L**	%
V1	184 ± 3	200 ± 4	7.6
V2	775 ± 6	800 ± 4	3.1
V_{1+2}	463 ± 4	500 ± 5	7.2

[1] Uncertainty calculated from error propagation from calibration curve.
[2] Uncertainty calculated from uncertainties on equipment used.

from V1 into the mixed solution. All validation readings are however within the 10% requirement of the OP (EPA, 2017).

4.2 Tracer study setup

4.2.1 Experiment 1

Although steady-state conditions were impossible, a method with constant inflow was suggested to minimize flow variables. Without rain, two alternatives for water flow through the system were evaluated. Ideally, water could be pumped from the domestic water distribution system. However, this would result in a waste of high volumes of good quality drinking water, which also came at a high cost. Since the storm water treatment system also functions as detention basins, large volumes of water were already available on site. It was determined that the other two settling tanks provide water as a flow source during the tracer study.

Without enough water in settling tank 1 and 2, a complete tracer output curve can not be produced. A complete analysis of retention time is thus not possible, but the data can still be used for a dispersion analysis.

4.2.2 Experiment 2

Experiment 2 was set up to measure natural, pulse-like rainfall events. This introduces some calculation limitations due to the variable nature, but it also includes the hydraulic behavior and dispersion during realistic conditions.

4.2.3 Operational conditions

Estimations for operational conditions of Experiment 1 and Experiment 2 are presented here, followed by a discussion of flow estimations. Finally, the results and discussion of flow regime is given.

Figure 4.3 show measured and calculated conditions with respect to inflow rate, outflow rate, mean system flow rate, nominal residence time, tracer mass introduced and corrections for background and temperature.

Background and temperature corrections

Although tap water was used as a calibration blank, storm water with increased turbidity may still present background levels of fluorescence. Before starting the tracer analysis, the background readings in the storm water must be determined and sensor readings should be adjusted accordingly (Wilson et al., 1986). In addition, the water temperature at the sampling site for the tracer analysis must be determined to correct for any temperature difference from the base temperature during calibration (T=20.2°C).

Table 4.3: *Calculated operational conditions for Experiment 1 and 2.*

	Exp. 1	**Exp. 2**	**Unit**
V_{sys}	113	86	m^3
Average Q_{in}	4.4	0.88	$10^{-3}\ m^3/s$
Average Q_out	2.0	0.90	$10^{-3}\ m^3/s$
Q_{mean}	3.2	0.89	$10^{-3}\ m^3/s$
t_n	589	1610	min
Δt	2	3	min
M_{in}	40	40	g
$\overline{RFU}_B$	0.36	2.2	RFU
ΔT	+10	+15	°C
T_{cf}	0.76	0.66	unitless

Flow estimations of Experiment 1

Estimations of the outflow rate with the Torricelli formula was controlled for by checking if total V_{out} was equivalent to total V_{in}, with acceptable results ($dV_{(in-out)^2} \approx 0$). Figure 4.3 shows the estimated Q_{out} in relation to Q_{in}. Ideally, when the tank was full, Q_{in} should equal Q_{out}. As can be seen by Figure 4.3, Q_{out} is steady at $0.0033m^3/s$, and not at $0.0044m^3/s(Q_{in})$. This distance could be due to errors in the use of Torricelli formula, overestimation of Q_{in} or instrumental errors in the depth measurements. It could also be due to the bypass of water when the system is in overflow. Torricellis formula only calculates the flow which passes through the 50 mm outlet pipe, and does not account for the water bypassing over the wall, and so Q_{out} may be underestimated. However, since V_{in} versus V_{out} shows an acceptable balance close to 0, the calculated Q_{out} is determined appropriate for further data analysis.

The average system velocity, υ, was calculated to be $7.85 \cdot 10^{-4}$ m/s, when based on mean system flow ($Q_{mean} = 0.0032m^3/s$) and the system volume ($V_{sys} = 113m^3$). Although the volume of the system changed over time, V_{sys} was determined by the tracer mass averaged volume, V_m (Eq. 2.35). These calculations do not take into account the variable nature of a non-steady flow system, but can nevertheless give some information on the flow regime (laminar or turbulent) and nominal residence time. It should be noted however, that the nominal residence time assumes steady-flow. With enough water, the system could have been brought into steady-state with a full tank, as seen in Figure 4.2. The water depth keeps rising until the system is in overflow, as can be seen by constant depth between 380 and 446 min. Here, the system should have steady-flow with $Q_{in} = Q_{out}$ which would have simplified the data analysis. Unfortunately, there was not enough water to pump after 446 min, and the water level can be seen declining in Figure 4.2. Between 232 and 246 min, the pump was stopped and moved from tank 3 to tank 2. The depth data, consequently the volume, clearly show the influence of the variable flow during the experiment.

Flow estimations of Experiment 2

Inflow rate obtained from flowmeter measurements appeared stable. Due to difficulties with the outlet flowmeter, outflow rate was estimated by the Torricelli formula as described above. Fluid velocity was determined for mean flow and volume given in Table 4.3, which gave a velocity of $2.87 \cdot 10^{-4}$ m/s.

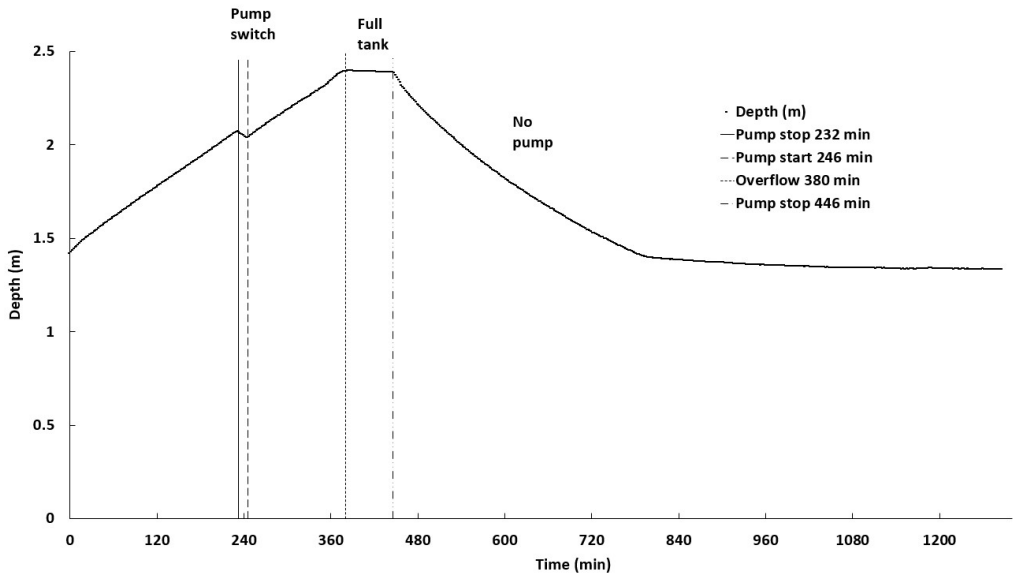

Figure 4.2: *Depth data from YSI-sensor during Experiment 1, with illustrated times for pump switch, full tank (overflow) and no pump.*

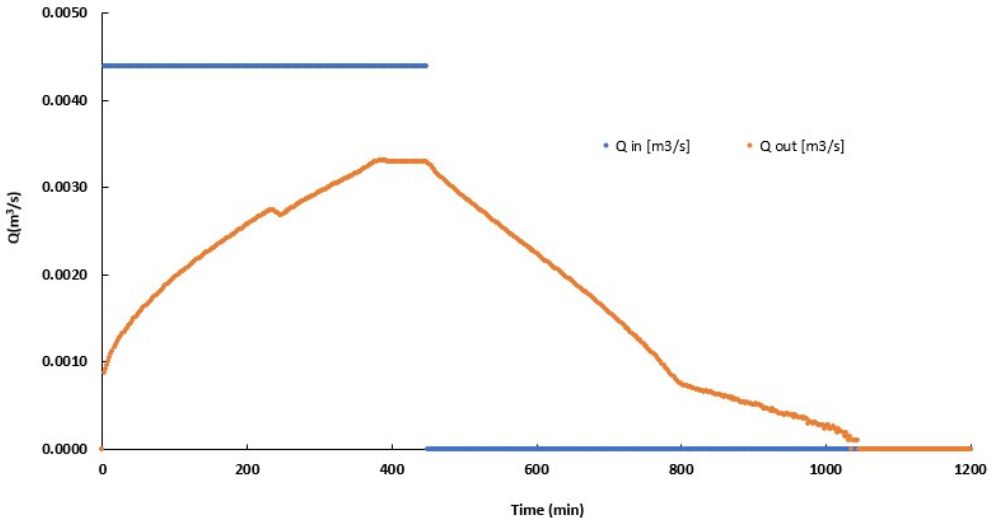

Figure 4.3: *Flow curve, with Q_{in} and Q_{out} plotted versus time.*

Flow regime

To evaluate if the flow regime was laminar or turbulent, N_R was determined for two conditions in Experiment 1; velocity at full tank conditions ($Q = 0.0044m^3/s$, $A = 4.52m^2$, ie. $\upsilon = 9.73 \cdot 10^{-4}m/s$), and average system velocity ($\upsilon = 7.85 \cdot 10^{-4}m/s$). For full tank conditions, N_R was calculated to be 445 (Eq. 2.15), and average velocity with open-channel flow gave a N_R of 1750 (Eq. 2.16). Both conditions fall within the range of transitional flow according to Tchobanoglous et al. (2014), but can still be considered laminar according to the limit generally accepted in the industry (Engineering ToolBox, 2004). For Experiment 2, mean operational conditions were used to find a N_R of 520, also in the laminar region. It should be noted, that the flowmeter registered some high inflow peaks ($Q_{in} = 0.017m^3/s$). Such high flowrates could influence the flow regime towards more turbulent conditions. It is possible these were alleviated by the 2500 mm manhole, prior to the sedimentation tank.

A flow regime with laminar conditions is preferred for particle removal by sedimentation. Sedimentation is enhanced with laminar conditions, as the particles entering the MSS will have increased settling velocity, due to the decreased drag coefficient (Åstebøl & Hvitved-Jacobsen, 2014; Tchobanoglous et al., 2014).

4.3 C-curves and qualitative analysis

Figure 4.4 and Figure 4.5 show the tracer output curves, or C-curves, for Experiment 1 and Experiment 2 respectively. There was not enough water in tank 3 and 2 for pumping to produce a complete tracer output in Experiment 1, and the experiment concluded at 1042 min, when Q_{out}=0. Some tracer dye was then left in the system.

The timing of switching tanks for the pump, full tank conditions can be seen marked in Figure 4.4. Interestingly, both instances of stopping the pump were followed by some increase in RWT concentration. Whether this is connected to the change in inflow or by other hydraulic conditions in the tank, is difficult to say.

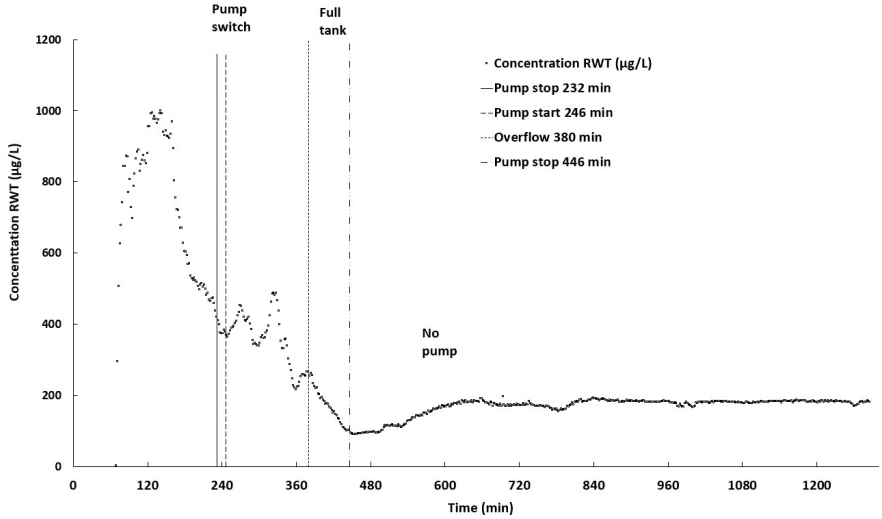

Figure 4.4: *Tracer output curve, or C-curve, for Experiment 1.*

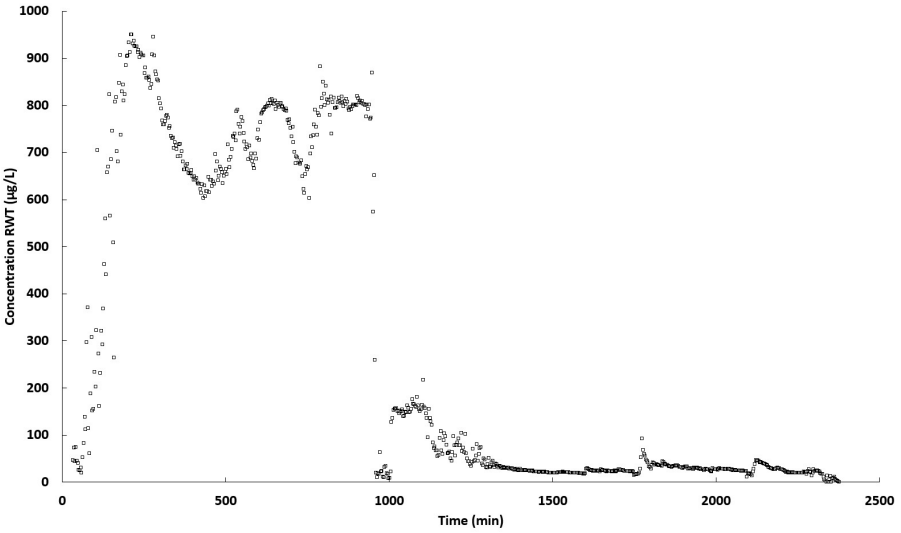

Figure 4.5: *Tracer output curve, or C-curve from Experiment 2.*

For Experiment 1, the C-curve shows a maximum concentration value of 998 μg/L. There is a rapid climb to the peak between 70 min and 142 min, before rapidly decreasing. Then, two smaller peaks are observed at 227 min and 328, followed by a long tail. According to Stephenson and Sheridan (2021), a long tail indicates dead-zones, whereby the tracer is temporarily stored before slowly released the outlet. The rapidly climbing peak and long tail could be interpreted as multiple flow processes. One is a rapid flow

signalling a plug flow effect with a short period of high tracer concentration, while the other compartment which was influences by mixing, flows more slowly, leading to the lower concentrations along the tail. The additional peaks could also indicate the presence of parallel flowpaths as well as internal recirculation (Levenspiel, 1999). These observations mainly concern C-curves under steady-flow conditions. As described for operational conditions, the MSS experienced variable inflow and outflow rate, as well as volume changes during the experiment, which will also influence the shape of the C-curve. A numerical analysis of the normalized response curve will help determine the presence of mixing, short-circuiting and presence of deadzones for variable flow conditions, and is presented later in this chapter.

Experiment 2 also experiences a rapid climb to the concentration peak of 950 μg/L at 213 min. The C-curve also decreases rapidly, but then experiences triple peaks at 537, 642 and 789 min, before declining into a long tail lasting approximately 1000 min (17 h). Similarly to Experiment 1, the visual inspection of the second C-curve may indicate dead-zones, mulitple flowpaths and internal recirculation. Due to the climatic effects of rainfall driven flow, the volume-based RTD analysis provides more robust understanding of the hydraulic behaviors of the MSS.

4.4 Method of moments analysis

Table 4.4 presents the calculated hydraulic characteristics of Experiment 1, according to the MOM technique on tracer data. Results from the MOM technique on data from the TIS-model is also included for comparison. Results from the MOM-technique modified with the volume-based RTD, for both experiments, are presented in Table 4.5.

The calculated tracer mass recovery was 84%, within the acceptable limit of 80% (Kadlec & Wallace, 2009). It should be noted, however, that the outgoing tracer mass is highly dependent on correct measurements of the discharge rate. If the calculated outflow rate is correct, then the quality of the tracer test is verified with the obtained tracer mass recovery. For the continued analysis, correct outflow estimations are presumed true.

In order to calculate t_n, the system is assumed to have "steady-flow", where Q_{mean} and V_{sys} give a t_n of 589 min. The total duration of the experiment was 1042 min, and t_m was calculated to be 402 min from the tracer data, while the TIS-model showed 225 min. This difference can be attributed to the long tail of the tracer data compared to the modelled TIS-curve. Both cases have a shorter t_m than t_n. Consequently, the effective volume ratio ($e = 0.73$) indicate a moderate amount of of dead zones from the tracer test, while the

TIS-model indicates a high amount of dead zones ($e = 0.40$) (Thackston et al., 1987). Effective volume ratio is directly dependent on t_n, which is calculated based on assumptions of steady-flow. For variable flow systems, such as the current study, the use of effective volume ratio is questionable. Alternative methods for hydraulic characterization of variable flow exists, and effective volume ratio is perhaps an example of a parameter of less importance in such systems.

The problem of non-uniform flow arises for the dispersion coefficients as well, as the equations involve the use of fluid velocity, which is variable according to the changing flow and cross-sectional area of fluid in the system. Nevertheless, the dispersion calculations for velocities given in Sections 4.2.3 and 4.2.3 could still give some indications of the dispersion conditions. Both the tracer data and TIS-model indicate moderate and high axial dispersion ($d > 0.05$), but within the lower end of the dispersion range given for rectangular sedimentation tanks (Tchobanoglous et al., 2014). Both Peclet numbers of 3.8 (tracer data) and 7.14(TIS) show a tendency towards advection being the main transport mechanism in the MSS.

It is evident from the tracer response curve that the MSS is neither an ideal CFSTR or PFR. The shape of the curve is better described by TIS conditions. The shape of the curve, as it deviates from ideal PFR, can be described by the mixing scale, represented by number of tanks in series, N (Levenspiel, 1999; Wahl et al., 2010). As listed in Table 4.4, N was 1.86 based on the tracer data, while the TIS-model gave a higher number of 3.46. An increased number of tanks-in-series, decreases the spread of the curve towards plug-flow conditions. The N obtained from tracer data, indicates the presence of relatively high mixing conditions in the MSS. Although the modelled curve was not a perfect fit with the tracer data ($SSQE = 1.0 \cdot 10^7$), it minimized the weight of the long tracer tail. The lower number N for tracer data, 1.86 could be due to the weight of the long tail in the tracer curve, with increased variance, in comparison with the TIS-model curve.

Lastly, it should be noted that Experiment 1 did not produce a complete C-curve. The calculated indices for hydraulic behavior and mean residence time are therefore not accurately determined by the incomplete data (Wahl et al., 2010). The TIS-model does however alleviate this in some degree by presenting an alternative tail function.

4.5 Model curves

The SSQE did not show a convincing result for evaluating the goodness-of fit between the LCF-models and the tracer output data. The two models

Table 4.4: *Hydraulic characteristics from Experiment 1, MOM.*

	Tracer data	**TIS-model**	**Unit**
MR	85	90	%
A_I	0.15	0.09	unitless
t_m	402	225	min
t_n	552	552	min
e	0.73	0.40	unitless
σ_c^2	86626	14742	min^2
σ_θ^2	0.54	0.29	unitless
d	0.26	0.14	unitless
D	0.003	0.002	m^2/s
P_e	3.8	7.14	unitless
N	1.86	3.46	unitless

with the best fit was the LCF-model $C(t)_{P,P}$ (planar in, planar out) and the TIS-model, seen as the green and blue curve, respectively, in Figure 4.6.

From a visual inspection, the initial tracer response looks to follow the sharp increase similar to the LCF-model. However, the LCF-model does not account for dispersion. The decline is due to the different velocities in the laminar parabolic flow profile. The TIS-model, on the other hand, include dispersion, represented by the variance of the distribution. It also minimizes the effect of the long tail on the variance, which is most likely caused by the decreasing flow rate after the pump stop. For dispersion analysis, the variance of the TIS-model might be more representative of how the tracer curve would appear had the system continued in steady-flow conditions. Both the laminar convenction model and the TIS-model produced a lower t_m than the tracer output data. Note, the LCF-model refers to an average t_m, while each fluid layer in the velocity profile holds a respective t_m represented by each point in the curve. Since the assumption of steady-flow does not hold true, a numerical analysis could at best give some indications, but the results would still be questionable.

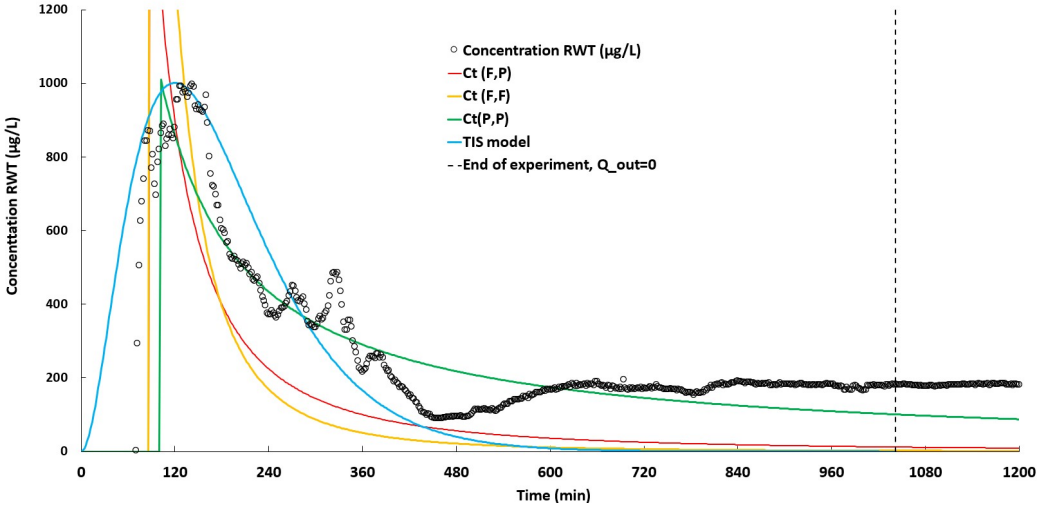

Figure 4.6: *Tracer response curve fitted with model curves:* $C(t)_{F,F}$, $C(t)_{F,P}$, $C(t)_{P,P}$ *and the TIS-model. The peaks of* $C(t)_{F,F}$ *and* $C(t)_{P,P}$ *are cutoff from the plot due to very high values (>3000 ug/L).*

4.6 Volume-based RTD analysis

The results of the volume-based RTD analysis are presented in Table 4.5. Both experiments show an acceptable ratio of tracer recovery with M_0^* close to 1 (Werner & Kadlec, 1996). M_1^* for both experiments have values well below 1, indicating short-circuiting with the presence of dead zones in the MSS(Holland et al., 2004). The M_2*-value, a measure of spread, was lower for Experiment 1 (M_2*=0.07) than Experiment 2 (M_2*=0.22). Both are above the ideal value of 0, indicating the presence of some longitudinal mixing, but to a higher effect in Experiment 2. The MI of the two experiments, 0.35 and 0.39, show potential for improved hydraulic behavior. In the work of Wahl et al. (2010), MI values were correlated ($R^2 = 0.94$) to pollutant removal by first-order reactions in constructed wetlands. Had the MSS been based on first-order reaction removal, the MI values of 0.35 and 0.39 would correspond to 30% removal. These findings are not comparable towards to the treatment efficiency of the MSS with gravitational settling as the primary removal mechanism. Even still, the findings of Wahl et al. (2010) is an example of how the MI relates poor hydraulic behavior to poor pollutant removal, and future studies should be conducted to find out if MI has a similar correlation to particle removal by sedimentation.

Table 4.5: *Zeroth (M_0^*), first (M_1^*) and second moment (M_2^*) , followed by the moment index (MI) from the volume-based RTD analysis.*

	Exp. 1	**Exp.2**
M_0^*	0.99	1.00
M_1^*	0.35	0.40
M_2^*	0.07	0.22
MI	0.35	0.39

In a comparison study of classic and volume based RTD analysis, Aylward et al. (2019) found a significant difference with the Student's T-test (95% confidence) of the results obtained from the two RTD methods. The study conclude the volume-based RTD analysis as the preferred method. It provides the possibility of universal comparison of tracer data for a range of systems with different flow conditions.

4.7 Influence of hydraulic behavior on sedimentation

The results from the tracer analysis all point towards non-ideal hydraulic behavior with the presence of mixing, longitudinal dispersion and short-circuiting with dead zones and potential multiple flow paths. Such hydraulic behavior has implications for optimal sedimentation, but to which degree is difficult to say without a simultaneous analysis of particle removal during the tracer studies. Although the obtained HRT will vary according to flow rate, an attempt was made to assess some theoretical settling times to compare to the HRT.

Table 4.6 shows the input values and terms used to calculate particle settling velocity. The drag coefficient C_d was determined by Equation 2.8, as the obtained N_R values for both experiments showed flow regime to be in the transitional region according Tchobanoglous et al. (2014). Since the use of Stoke's Law is not appropriate for $N_R > 1$, Newton's Law (Eq. 2.5) was used to determine the settling velocity. Li et al. (2008) suggested that wet specific gravity is a more reasonable parameter than dry specific gravity, and found wet specific gravity of stormwater particles in the range of 1.30 to 1.42, with an average of 1.35. The average of 1.35 was selected for settling velocity determination. The height used in Equation 2.12 was determined from the

Table 4.6: *Calculation terms and resulting settling velocity (v_p) and settling time (t_s).*

	Experiment 1	**Experiment 2**	**Unit**
N_R	1750	520	unitless
C_d	0.43	0.51	unitless
d_p	0.45	0.45	10^{-6}m
sg_p	1.35	1.35	unitless
v_p	2.2	2.0	10^{-3}m/s
H	0.68	0.21	m
t_s	5.1	1.75	min

height difference between system water levels (based on V_{sys}) and the level of the outlet at 1.35 m.

Settling velocities for the given conditions in Experiment 1 and 2 were calculated to be 5.1 and 1.75 min, respectively. Then, the mean residence time of 408 min for Experiment 1 gave more than enough time for particle settling. However, Li et al. (2008) reported experimental settling velocities to be much lower than those calculated from Newton's law. One should be mindful of determining settling efficiency of a system purely based on residence time and settling velocity calculations. Not to mention, as a detention basin, the MSS is designed to experience large depth fluctuations and so the height used for settling time determination cannot be a fixed value as used above. Lastly, variable natural flow rates prevents the use of HRT as the main treatment design factor for stormwater detention tanks.

If the settling time and range of residence times should be in the same order of magnitude as the calculations above, treatment performance would be relatively high in most cases. However, previous studies show that the performance may be as low as 48 % (Bergseng, 2021), which could suggest these settling times are much lower, or heavily affected by the hydraulic behavior within the tank. In addition, Bergseng (2021) found indications of particle re-suspension, when one of the tests showed a rise of pH, electrical conductivity, turbidity and increased particulate Zn from inflow to outflow. She also found that particles skewed towards larger particles in the outflow. Re-suspended particles in the outflow could be even more detrimental to the environment than the influent stormwater. It is essential to establish at which

flow conditions such re-suspension occurs, and should be followed up by a bypass installation as a protection measure.

Indices determined from the tracer analysis, could have the potential to influence design factor. Persson et al. (1999) used the λ parameter of hydraulic efficiency, described by e and N to compare different shapes and inlet/outlet configurations of constructed wetlands, and later on tried to relate these indices to removal efficiency of nitrogen (Persson & Wittgren, 2003). The authors noted, however, that it may not be appropriate to give e and N the same weight. Although convenient to calculate, Holland et al. (2004) advised caution with the λ index, as it is especially susceptible to error when the RTD is not smooth. With e dependent on a nominal retention time, the variable flow and volume conditions of stormwater detention tanks makes it an even more inappropriate index. The MI on the other hand, was shown to have a much higher correlation with pollutant removal with an R^2 value of 0.94, while the hydraulic efficiency proposed by Persson et al. (1999) had an R^2 of 0.41 (Wahl et al., 2010). Both indices were used to examine correlation with nutrient removal. To the authors knowledge, limited studies have been done to investigate how λ and MI correlate with pollution removal by sedimentation.

An index of hydraulic behavior capable of connecting different design configurations with removal rate of suspended solids, would substantially aid in developing design guidelines for stormwater detention tanks.

4.8 Limitations of this study

The full scale tracer study came with some practical limitations which affected the quality of the results. These limitations are listed below.

- Water access for constant inflow was limited, which made it difficult to achieve steady-state conditions. The MOM-analysis, TIS- and LCF-models and the qualitative analysis are based on the assumption of steady-state. The methods were still applied for analysis, but with non-steady flow conditions, the results are merely indicative.

- The challenge of limited water access for constant inflow made replication of Experiment 1 impossible. Experiment 2 relied on variable rainfall events to produce a complete RTD curve, and the ensuing long and unpredictable time frame also ruled out the possibility of replication. Thus, a statistical analysis was excluded in this project.

- This project described the hydraulic behavior of the MSS, but not how it relates to TSS removal rates. Analysis of particle removal combined with

the tracer studies would most likely have exceeded the time limitations for this project.

- Technical constraints limited the quality of data, as the the tracer data analysis depends heavily on measurements of flow (EPA, 2002). The estimated outflow rate may not represent the true outflow rate.

4.9 Suggestions for future studies

Listed below are ideas for possible future work.

- Future studies should look into which flow conditions and associated hydraulic behavior re-suspension occurs. This could possibly be done by joining tracer studies for hydraulic behavior with simultaneous removal rate experiments for suspended solids.

- Hydraulic behavior indices which could describe design configurations and removal of suspended solids, such as MI, should be further tested across several systems. Determination and validation of such an index would substantially aid in developing appropriate design guidelines for stormwater detention tanks for optimising treatment performance.

- Time for sedimentation is dependent upon settling height. In a stormwater detention tank such as the MSS, settling height may vary according to the filling and emptying of the tank. What does it mean for sedimentation efficiency? Is there an optimum design whereby the volume may increase for detention purposes, while still ensuring minimal depth fluctuations?

- Only one tank was tested - all three should be characterised for hydraulic behavior, as each is installed with two dividing walls at different lengths from the inlet. The hydraulic behavior should be compared with respect to positioning of dividing wall and removal rate. Similar studies have been done for constructed wetlands, when comparing shape and inlet/outlet configurations with respect to mixing and removal rates (Persson et al., 1999).

5. Conclusion

In this thesis, two tracer tests have been used to determine the hydraulic behavior of the MSS, a stormwater detention system designed for both flood protection and pollutant removal. Literary findings show that design features of a system influences the hydraulic behavior, which subsequently affect the settling efficiency of particles in stormwater. Since system design is based on a "Best Available Technology" principle, increased knowledge about the hydraulic behavior can contribute to improved technology for pollutant removal.

The results from Experiment 1 and 2 should be treated with caution due to the questionable quality of the tracer studies and no possibility for statistical analysis. Due to errors with the outflow measurement instrument, an attempt was made to estimate flow data using the Toricelli equation. However, this is an inherently uncertain method as it does not represent the real world outflow. Thus the ensuing outflow estimations challenge the calculated tracer mass recovery. Flow regime determination, the qualitative curve analysis, the MOM-technique and TIS-model results are conflicted by the inaccurate assumption of steady-state, and are indicative at best.

According to N_R calculations, the MSS flow regime is in the laminar region, with N_R values ranging from 445 to 1750. Laminar conditions are preferred for enhanced settling of particles.

A visual inspection of both C-curves suggest the presence of dead-zones, multiple flow paths and internal recirculation. However, changes in the shape of the C-curves could also be attributed to the variable flowrate of the system.

The MOM-technique and TIS-model for Experiment 1 show variable results for hydraulic residence time, 408 and 225 min, respectively. These are both lower than the estimated nominal residence time of 552 min (assuming steady-state), which can be attributed to short-circuiting with moderate amounts of deadzones ($e = 0.75$). In addition, the tracer curve variance display high axial dispersion (d=0.26) along with advection as the main transport mechanism ($P_e > 1$). The variance from the tracer data also constitutes high mixing conditions (N=1.86), but this could be due to the weight of the long tail. The TIS-model reduced this effect (N=3.46), which could mean the tracer data overestimates degree of mixing.

The volume-based RTD analysis is also indicative of short-circuiting, with M_1^* of 0.35 and 0.40 for Experiment 1 and 2, respectively. M_2^* point toward some degree of longitudinal mixing, but more so in Experiment 2 (Exp. 1 M_2^*=0.07, Exp.2 M_2^*=0.22). MI-values (0.35-0.39) are of limited use until further studies are conducted to properly link MI to removal rate of

settling solids. Such a linkage would be particularly meaningful for design considerations, in contrast to the hydraulic residence time parameter which may vary by magnitudes greater than those tested in this thesis. The results from the volume-based RTD analysis are more reliable than the preceding methods, being less affected by non-steady state conditions. Still, the challenge of non-precise outflow measurements remains.

All results point toward short-circuiting and longitudinal mixing in the MSS, which can reduce sedimentation efficiency. Further studies should be conducted to confirm these findings and to determine which design features could improve hydraulic behavior. Volume-based RTD analysis should be used to characterise stormwater detention tanks with variable flow, to further update "Best Available Technology" for design. This will aid in the process of optimising treatment of stormwater runoff and thus better protect the environment in receiving waters.

References

Åstebøl, S. O., & Hvitved-Jacobsen, T. (2014). *Water protection in road planning and road building* (No. 295). Norwegian Public Roads Administration. https://hdl.handle.net/11250/2658960

Aylward, L., Bonner, R., Sheridan, C., & Kappelmeyer, U. (2019). Hydraulic study of a non-steady horizontal sub-surface flow constructed wetland during start-up. *Science of the Total Environment*, *646*, 880–892. https://doi.org/10.1016/j.scitotenv.2018.07.324

Baek, D., Seo, I., Kim, J., & Nelson, J. (2019). UAV-based measurements of spatio-temporal concentration distributions of fluorescent tracers in open channel flows. *Advances in Water Resources*, *127*, 76–88. https://doi.org/10.1016/j.advwatres.2019.03.007

Behrens, H., Beims, U., Dieter, H., Dietze, G., Eikmann, T., Grummt, T., Hanisch, H., Henseling, H., Käß, W., Kerndorff, H., Leibundgut, C., Müller-Wegener, U., Rönnefahrt, I., Scharenberg, B., Schleyer, R., Schloz, W., & Tilkes, F. (2001). Toxicological and ecotoxicological assessment of water tracers. *Hydrogeology Journal*, *9*(3), 321–325. https://doi.org/10.1007/s100400100126

Bencala, K., Rathbun, R., Jackman, A., Kennedy, V., Zellweger, G., & Avanzino, R. (1983). Rhodamine WT dye losses in a mountain stream environment. *JAWRA Journal of the American Water Resources Association*, *19*(6), 943–950. https://doi.org/10.1111/j.1752-1688.1983.tb05944.x

Bergseng, K. (2021). *Performance of closed particle removal systems for treatment of road runoff* (Master Thesis). Norges teknisk-naturvitenskapelige universitet. https://hdl.handle.net/11250/2991801

Bodin, H., Mietto, A., Ehde, P. M., Persson, J., & Weisner, S. E. B. (2012). Tracer behaviour and analysis of hydraulics in experimental free water surface wetlands. *Ecological Engineering*, *49*, 201–211. https://doi.org/10.1016/j.ecoleng.2012.07.009

Bodin, H., Persson, J., Englund, J.-E., & Milberg, P. (2013). Influence of residence time analyses on estimates of wetland hydraulics and pollutant removal. *Journal of Hydrology*, *501*, 1–12. https://doi.org/10.1016/j.jhydrol.2013.07.022

Center for Biologics Evaluation and Research. (2021). Validation of analytical procedures: Text and methodology guidance for industry. U.S Food; Drug Administration. https://www.fda.gov/media/152208/download

Clark, D., Lenain, L., Feddersen, F., Boss, E., & Guza, R. (2014). Aerial imaging of fluorescent dye in the near shore. *Journal of Atmospheric*

and Oceanic Technology, *31*(6), 1410–1421. https://doi.org/10.1175/JTECH-D-13-00230.1

Cox, M. H., Mendez, G. O., Kratzer, C. R., & Reichard, E. G. (2003). *Evaluation of tracer tests completed in 1999 and 2000 on the upper santa clara river, los angeles and ventura counties, california* (USGS Numbered Series No. 2003-4277). U.S. Geological Survey. Retrieved November 3, 2022, from http://pubs.er.usgs.gov/publication/wri034277

Danckwerts, P. (1953). Continuous flow systems. distribution of residence times. *Chemical Engineering Science*, *2*(1), 1–13. https://doi.org/10.1016/0009-2509(53)80001-1

Dierberg, F., & DeBusk, T. (2005). An evaluation of two tracers in surface-flow wetlands: Rhodamine-WT and lithium. *Wetlands*, *25*(1), 8–25. https://doi.org/10.1672/0277-5212(2005)025[0008:AEOTTI]2.0.CO;2

Droste, R. L., & Gehr, R. L. (2019). *Theory and practice of water and wastewater treatment* (2nd ed.). Hoboken, NJ, USA, Wiley. Retrieved December 27, 2022, from https://search.ebscohost.com/login.aspx?direct=true&db=nlebk&AN=1863402&scope=site

EC. (2018). *Technical guidance for deriving environmental quality standards. guidance document no: 27.* European Commision. Brussels, Belgium.

Engineering ToolBox. (2004). *Laminar, transitional and turbulent flow.* https://www.engineeringtoolbox.com/laminar-transitional-turbulent-flow-d_577.html

EPA. (1986). *Design manual municipal wastewater disinfection.* U.S Environmental Protection Agency. https://www.wbdg.org/FFC/EPA/EPACRIT/epa625_1_86_021.pdf

EPA. (2002). The QTRACER2 program for tracer-breakthrough curve analysis for tracer tests in karstic aquifers and other hydrologic systems. U.S Environmental Protection Agency. https://cfpub.epa.gov/si/si_public_record_report.cfm?Lab=NCEA&dirEntryId=54930

EPA. (2017). *Operating procedure for dye tracer measurements.* U.S Environmental Protection Agency. Athens, Georgia.

Everts, C., & Kanwar, R. (1994). Evaluation of rhodamine WT as an adsorbed tracer in an agricultural soil. *Journal of Hydrology*, *153*(1), 53–70. https://doi.org/10.1016/0022-1694(94)90186-4

Fall, C., Flores-Alamo, N., Esparza-Soto, M., & Hooijmans, C. (2012). Tracer test and hydraulics modeling of a large WWTP. *Water Practice and Technology*, *7*(1). https://doi.org/10.2166/wpt.2012.013

Fernald, A., Wigington, P., & Landers, D. (2001). Transient storage and hyporheic flow along the willamette river, oregon: Field measurements

and model estimates. *Water Resources Research*, *37*(6), 1681–1694. https://doi.org/10.1029/2000WR900338

Field, M. (2020). On tracer breakthrough curve dataset size, shape, and statistical distribution. *Advances in Water Resources*, *141*. https://doi.org/10.1016/j.advwatres.2020.103596

Field, M., Wilhelm, R., Quinlan, J., & Aley, T. (1995). An assessment of the potential adverse properties of fluorescent tracer dyes used for groundwater tracing. *Environmental Monitoring and Assessment*, *38*(1), 75–96. https://doi.org/10.1007/BF00547128

Gausel Lode, M. (2021). *Road runoff particle removal: A case study of the underground sedimentation facility at fv. 505 skjæveland – foss-eikeland* (Master Thesis). University of Stavanger.

Gooseff, M., LaNier, J., Haggerty, R., & Kokkeler, K. (2005). Determining in-channel (dead zone) transient storage by comparing solute transport in a bedrock channel-alluvial channel sequence, oregon. *Water Resources Research*, *41*(6), 1–7. https://doi.org/10.1029/2004WR003513

Guo, C., Cui, Y., Shi, Y., Luo, Y., Liu, F., Wan, D., & Ma, Z. (2019). Improved test to determine design parameters for optimization of free surface flow constructed wetlands. *Bioresource Technology*, *280*, 199–212. https://doi.org/10.1016/j.biortech.2019.02.020

Headley, T. R., & Kadlec, R. H. (2007). Conducting hydraulic tracer studies of constructed wetlands: A practical guide. *Ecohydrology & Hydrobiology*, *7*(3), 269–282. https://doi.org/10.1016/S1642-3593(07)70110-6

Hoffman, E., Latimer, J., Hunt, C., Mills, G., & Quinn, J. (1985). Stormwater runoff from highways. *Water, Air, and Soil Pollution*, *25*(4), 349–364. https://doi.org/10.1007/BF00283788

Holcová, V., Šíma, J., Edwards, K., Semančíková, E., Dušek, J., & Šantrůčková, H. (2009). The effect of macrophytes on retention times in a constructed wetland for wastewater treatment. *International Journal of Sustainable Development & World Ecology*, *16*(5), 362–367. https://doi.org/10.1080/13504500903201146

Holland, J., Martin, J., Granata, T., Bouchard, V., Quigley, M., & Brown, L. (2004). Effects of wetland depth and flow rate on residence time distribution characteristics. *Ecological Engineering*, *23*(3), 189–203. https://doi.org/10.1016/j.ecoleng.2004.09.003

Innst. S. nr. 183 (2006-2007). (n.d.). *Vern av villaksen og ferdigstilling av nasjonale laksevassdrag og laksefjorder*.

Johansen, K., Dunne, A. F., Tu, Y.-H., Almashharawi, S., Jones, B. H., & McCabe, M. F. (2022). Dye tracing and concentration mapping in coastal waters using unmanned aerial vehicles. *Nature Publishing Group*, *12*(1), 1141. https://doi.org/10.1038/s41598-022-05189-9

Kadlec, R. H., & Wallace, S. D. (2009). *Treatment wetlands* (2nd ed.). Boca Raton (Fla.), CRC press.

Kasnavia, T., Vu, D., & Sabatini, D. (1999). Fluorescent dye and media properties affecting sorption and tracer selection. *Ground Water*, *37*(3), 376–381. https://doi.org/10.1111/j.1745-6584.1999.tb01114.x

Keefe, S., Barber, L., Runkel, R., Ryan, J., McKnight, D., & Wass, R. (2004). Conservative and reactive solute transport in constructed wetlands. *Water Resources Research*, *40*(1), W012011–W0120112. https://doi.org/10.1029/2003WR002130

Kommedal, R. (2020). *Physical unit operations* (Lecture) [Lecture]. University of Stavanger.

Kommedal, R. (2022). Reactor characterization lab manual. University of Stavanger.

Lavrnić, S., Alagna, V., Iovino, M., Anconelli, S., Solimando, D., & Toscano, A. (2020). Hydrological and hydraulic behaviour of a surface flow constructed wetland treating agricultural drainage water in northern italy. *Science of The Total Environment*, *702*, 134795. https://doi.org/10.1016/j.scitotenv.2019.134795

Ledje, U. P., & Randulff, S. T. (2019). *Helhetlig tiltaksplan for figgjovassdraget, rogaland* (Ecofact rapport: 687). Sandnes Kommune. https://www.gjesdal.kommune.no/_f/p21/i19ad22f6-8e09-4183-8691-ba52fd1e4f07/helhetlig-tiltaksplan-for-figgjovassdraget-rogaland.pdf

Levenspiel, O. (1999). *Chemical reaction engineering* (3rd ed.). New York, Wiley.

Li, Y., Kang, J.-H., Lau, S.-L., Kayhanian, M., & Stenstrom, M. (2008). Optimization of settling tank design to remove particles and metals. *Journal of Environmental Engineering*, *134*(11), 885–894. https://doi.org/10.1061/(ASCE)0733-9372(2008)134:11(885)

Li, Y., Lau, S.-L., Kayhanian, M., & Stenstrom, M. (2005). Particle size distribution in highway runoff. *Journal of Environmental Engineering*, *131*(9), 1267–1276. https://doi.org/10.1061/(ASCE)0733-9372(2005)131:9(1267)

Lin, A.-C., Debroux, J.-F., Cunningham, J., & Reinhard, M. (2003). Comparison of rhodamine WT and bromide in the determination of hydraulic characteristics of constructed wetlands. *Ecological Engineering*, *20*(1), 75–88. https://doi.org/10.1016/S0925-8574(03)00005-3

Marsalek, J., Oberts, G., Exall, K., & Viklander, M. (2003). Review of operation of urban drainage systems in cold weather: Water quality considerations. *Water Science and Technology*, *48*(9), 11–20. https://doi.org/10.2166/wst.2003.0481

Meland, S. (2010). *Ecotoxicological effects of highway and tunnel wash water runoff* (Doctoral dissertation). Norwegian University of Life Sciences. Ås. http://hdl.handle.net/11250/2431910

Mukherjee, A., Fryar, A., & Lasage, D. (2005). Using tracer tests to assess natural attenuation of contaminants along a channelized coastal plain stream. *Environmental and Engineering Geoscience*, *11*(4), 371–382. https://doi.org/10.2113/11.4.371

National Center for Biotechnology Information. (2022). *PubChem compound summary for CID 37718, rhodamine WT.* [National center for biotechnology information]. Retrieved October 29, 2022, from https://pubchem.ncbi.nlm.nih.gov/compound/Rhodamine-WT

Nix, S. J. (1985). Residence time in stormwater detention basins. *Journal of Environmental Engineering*, *111*(1), 95–100. https://doi.org/10.1061/(ASCE)0733-9372(1985)111:1(95)

Norsk Vann. (2020). Kommunaltekniske normer for vann- og avløpsanlegg. vedlegg 9. overvannshåndtering sandnes kommune. VA-norm. http://www.va-norm.no/wp-content/uploads/2020/12/Vedlegg-9-Overvannshandtering.pdf

NPRA. (2018). *Vegbygging NORMAL [håndbok n200].* Norwegian Public Roads Administration. https://hdl.handle.net/11250/2760702

Ødegaard, H. (2014). *Vann- og avløpsteknikk* [OCLC: 939782945]. Hamar, Norsk Vann.

Parker Jr, G. (1973). Tests of rhodamine WT dye for toxicity to oysters and fish. *J.RES.US GEOL.SURV.*, *1*(4), 499. https://www.scopus.com/inward/record.uri?eid=2-s2.0-0015900998&partnerID=40&md5=085f92480a62e14e6d5a580afc715a9f

Persson, J., Somes, N., & Wong, T. (1999). Hydraulics efficiency of constructed wetlands and ponds. *Water Science and Technology*, *40*(3), 291–300. https://doi.org/10.1016/S0273-1223(99)00448-5

Persson, J., & Wittgren, H. B. (2003). How hydrological and hydraulic conditions affect performance of ponds. *Ecological Engineering*, *21*(4), 259–269. https://doi.org/10.1016/j.ecoleng.2003.12.004

Raimondi, A., & Becciu, G. (2017). On the efficiency of stormwater detention tanks in pollutant removal. *International Journal of Sustainable Development and Planning*, *12*(1), 144–154. https://doi.org/10.2495/SDP-V12-N1-144-154

Research Council of Norway. (2019). *RENTVEGVANN: New multistage concept for treatment of road water* (No. 296325). Research Council of Norway. https://prosjektbanken.forskningsradet.no/project/FORISS/296325

Rivord, J., Laurel Saito, P., Miller, G., & Stoddard, S. (2014). Modeling contaminant spills in the truckee river in the western united states. *Journal of Water Resources Planning and Management*, *140*(3), 343–354. https://doi.org/10.1061/(ASCE)WR.1943-5452.0000338

Rowiński, P., & Chrzanowski, M. (2011). Influence of selected fluorescent dyes on small aquatic organisms. *Acta Geophysica*, *59*(1), 91–109. https://doi.org/10.2478/s11600-010-0024-7

Rowiński, P., Guymer, I., & Kwiatkowski, K. (2008). Response to the slug injection of a tracer - a larger-scale experiment in a natural river. *Hydrological Sciences Journal*, *53*(6), 1300–1309. https://doi.org/10.1623/hysj.53.6.1300

Ruehl, C., Fisher, A., Hatch, C., Huertos, M., Stemler, G., & Shennan, C. (2006). Differential gauging and tracer tests resolve seepage fluxes in a strongly-losing stream. *Journal of Hydrology*, *330*(1), 235–248. https://doi.org/10.1016/j.jhydrol.2006.03.025

Runkel, R. L. (2015). On the use of rhodamine WT for the characterization of stream hydrodynamics and transient storage. *Water Resources Research*, *51*(8), 6125–6142. https://doi.org/10.1002/2015WR017201

Sabatini, D., & Austin, T. (1991). Characteristics of rhodamine WT and fluorescein as adsorbing ground-water tracers. *Groundwater*, *29*(3), 341–349. https://doi.org/10.1111/j.1745-6584.1991.tb00524.x

Shiau, B., Sabatini, D., & Harwell, J. (1993). Influence of rhodamine WT properties on sorption and transport in subsurface media. *Groundwater*, *31*(6), 913–920. https://doi.org/10.1111/j.1745-6584.1993.tb00864.x

Skjolding, L., Jørgensen, L., Dyhr, K., Köppl, C., McKnight, U., Bauer-Gottwein, P., Mayer, P., Bjerg, P., & Baun, A. (2021). Assessing the aquatic toxicity and environmental safety of tracer compounds rhodamine b and rhodamine WT. *Water Research*, *197*. https://doi.org/10.1016/j.watres.2021.117109

Smart, P., & Laidlaw, I. (1977). An evaluation of some fluorescent dyes for water tracing. *Water Resources Research*, *13*(1), 15–33. https://doi.org/10.1029/WR013i001p00015

Smith, S. A. (2019). How algae sensors work. YSI, Webinar. https://www.ysi.com/webinars/how-algae-sensors-work-principles-and-practice-webinar

Smith, S. A. (2021). *Water quality monitoring with rhodamine* [YSI]. Retrieved December 11, 2022, from https://www.ysi.com/ysi-blog/water-blogged-blog/2020/04/what-is-rhodamine-get-the-rho-down

Stephenson, R., & Sheridan, C. (2021). Review of experimental procedures and modelling techniques for flow behaviour and their relation to residence

time in constructed wetlands. *Journal of Water Process Engineering*, *41*, 102044. https://doi.org/10.1016/j.jwpe.2021.102044

Storm Aqua AS. (2021). *FV505 renseanlegg for vegvann. renseløsning - systembeskrivelse som-bygget* (Technical report). Sandnes.

Sukhodolov, A. N., Nikora, V. I., Rowiński, P. M., & Czernuszenko, W. (1997). A case study of longitudinal dispersion in small lowland rivers. *Water Environment Research*, *69*(7), 1246–1253. Retrieved January 30, 2023, from https://www.jstor.org/stable/25044992

Tai, D., & Rathbun, R. (1988). Photolysts of rhodamine-WT dye. *Chemosphere*, *17*(3), 559–573. https://doi.org/10.1016/0045-6535(88)90031-8

Taylor, J. R. (1997). *An introduction to error analysis: The study of uncertainties in physical measurements* (2nd ed.). Sausalito, Calif, University Science Books.

Tchobanoglous, G., Stensel, D. H., Tsuchihashi, R., Burton, F., Abu-Orf, M., Bowden, G., & Pfrang, W., eds. *Wastewater engineering: Treatment and resource recovery* (5th ed.). 5th ed. New York: McGraw-Hill Education, 2014. ISBN: 978-0-07-340118-8.

Thackston, E., Shields, F., Jr., & Schroeder, P. (1987). Residence time distributions of shallow basins. *Journal of Environmental Engineering (United States)*, *113*(6), 1319–1332. https://doi.org/10.1061/(ASCE)0733-9372(1987)113:6(1319)

UN-Water. (2019). *Climate change and water UN-water policy brief*. United Nations. https://www.unwater.org/sites/default/files/app/uploads/2019/10/UN_Water_PolicyBrief_ClimateChange_Water.pdf

Vannforskriften. (2006). *Forskrift om rammer for vannforvaltningen* (FOR-2006-12-15-1446). Lovdata. https://lovdata.no/forskrift/2006-12-15-1446

Wahl, M. D., Brown, L. C., Soboyejo, A. O., Martin, J., & Dong, B. (2010). Quantifying the hydraulic performance of treatment wetlands using the moment index. *Ecological Engineering*, *36*(12), 1691–1699. https://doi.org/10.1016/j.ecoleng.2010.07.014

Werner, T. M., & Kadlec, R. H. (1996). Application of residence time distributions to stormwater treatment systems. *Ecological Engineering*, *7*(3), 213–234. https://doi.org/10.1016/0925-8574(96)00013-4

Werner, T. M., & Kadlec, R. H. (2000). Wetland residence time distribution modeling. *Ecological Engineering*, *15*(1), 77–90. https://doi.org/10.1016/S0925-8574(99)00036-1

Westerlund, C., & Viklander, M. (2006). Particles and associated metals in road runoff during snowmelt and rainfall. *Science of the Total*

Environment, *362*(1), 143–156. https://doi.org/10.1016/j.scitotenv.2005.06.031

Wilson, J. F., Cobb, E. D., & Kilpatrick, F. A. (1986). *Fluorometric procedures for dye tracing*. Department of the Interior, U.S. Geological Survey.

Writer, J., Ryan, J., Keefe, S., & Barber, L. (2012). Fate of 4-nonylphenol and 17beta-estradiol in the redwood river of minnesota. *Environmental Science and Technology*, *46*(2), 860–868. https://doi.org/10.1021/es2031664

YSI. (2020). *EXO user manual*. XYLEM. Yellow Springs, Ohio. https://www.ysi.com/file%20library/documents/manuals/exo-user-manual-web.pdf

6. Appendix

A: Instrument Calibration and validation

The calibration curve for standard solution D2-D9 is shown in Figure 6.1. The coefficient of determination, R^2, was calculated to be 0.999, which shows a strong linear relationship between measured fluorescence and RWT concentration. The regression line is represented by a slope and y-intercept, and their uncertainties are listed in Table 6.1. The regression line was used to calculate RWT concentrations during tracer experiments from fluorescence (RFU) measurements.

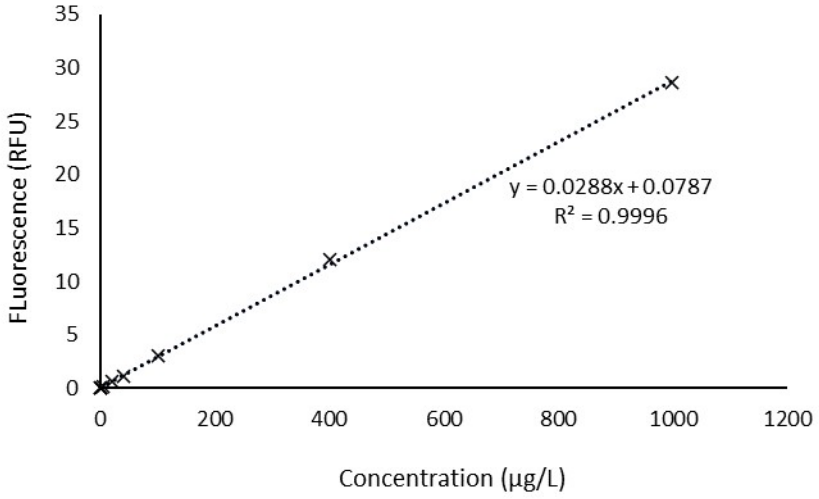

Figure 6.1: *Calibration curve with fluorescence, RFU, plotted against standard concentrations of Rhodamine WT, $\mu g/L$*

Table 6.1: *Regression analysis of calibration curve.*

Regression line variables	**Value**	**Standard deviation**	**Uncertainty (95 % conf. interval)**
Slope	0.0288	0.0002	± 0.0005
Y-intercept	0.0787	0.0823	±0.1946

Calibration procedure

The lab procedure for instrument calibration is described in the following section.

Materials

- Rhodamine WT 20 % (w/v, Thermo Fisher Scientific, VWR: cat. no 446970010)
- Volumetric flasks of 500 and 1000 mL and 25 mL bulb pipette
- Finnpipette F2 Variable Volume (Finntip 5 mL, Thermo Scientific)
- EXO1 sonde with TAL-PC and Temperature sensor (YSI,Inc.)
- Exo Handheld Display (YSI, Inc.)

Procedure

1. Identify blanks: Tap water was used for the calibration blank. Correct for negative background of distilled water which was used for dilution.
2. Prepare standard solutions as listed in Table 6.2.
3. Add 250 mL of each solution to the EXO1 calibration cup.
4. Immerse EXO1 sensor in solution for 1 minute to obtain consistent fluorescence and temperature reading.
5. Record fluorescence and temperature from the EXO Handheld Display.
6. Correct fluorescence readings for background and temperature.
7. Plot fluorescence and standard solutions in a calibration curve and determine regression line, uncertainty and limit of detection by applying the Excel linear regression analysis function.
8. Prepare validation RWT solutions of 200 μg/L and 800 μg/L. Mix the two solutions to obtain 500 μg/L.
9. Perform step 3-6 as described above and compare to the linear regression of the calibration curve,
10. Check validation with the 10 % validation requirement (EPA, 2017).

Dilution details

Formula for dilution calculation:

$$C_1V_1 = C_2V_2 \tag{6.1}$$

where C_2 is the concentration of final solution, V_2 is the volume of final solution and C_1 is the initial working standard solution.

First, a strong working standard was prepared by pipetting 1.0 mL RWT 20% in 999 mL distilled water. 50 mL from this solution was then pipetted into 950 mL distilled water to obtain the strong working standard of 1000mL with 10 000 μg/L. Four solutions (D2-D5) were then prepared by pipetting the strong working standard into 500 mL volumetric flasks, which were filled with distilled water. The solution of 100 μg/L was used further as a weak working standard to prepare an additional four low concentration solutions (D6-D9). Concentrations of all nine calibration solutions are given in Table 1, along with dilution volumes and concentrations.

Table 6.2: *Standard RWT solutions for analysis (C_2) with dilution volumes and concentrations.*

Short name	**C_2 (μg/L)**	**C_2 mg/L**	**V_2 mL**	**V_1 mL**	**C_1 mg/L**
Strong WST, D1	10000	10	1000	1	200
D2	1000	1	500	50	10
D3	400	0.4	500	50	10
Weak WST D4	100	0.1	1000	10	10
D5	40	0.04	500	2	10
D6	20	0.02	500	100	0.1
D7	4	0.004	500	20	0.1
D8	0.8	0.0008	500	4	0.1
D9	0.2	0.0002	500	1	0.1

C: Tracer study setup

(a) *Pump used to drive inlet flow*

(b) *Pump cable from manhole of tank 3*

Figure 6.2: *Pump setup for experiment 1 - The pump (a) was lowered into tank 3 with a rope, and the cable transported water out from tank 3 (b)*

(a) *Pump cable positioning to avoid angles for smooth flowthrough*

(b) *Pump cable into inlet chamber*

Figure 6.3: *Pump setup for experiment 1 - The cable had to be positioned to avoid angles for smooth flowthrough (a) of water into inlet chamber (b)*

(a) *YSI probe secured on a steel pole*

(b) *YSI probe lowered toward outlet pipe*

Figure 6.4: *YSI probe setup for sampling*

D: Tracer study analysis

t	V_{sys}	Real depth	V(t)	Q_{out}	C(t)	m_{out}	$V_t(t)$	ϕ	C'(ϕ)	C'(ϕ) x Δϕ	C'(ϕ) x ϕ x Δϕ	(ϕ-M1*)2 x C'(ϕ) x Δϕ
(min)	(m^3)	(m)	(m^3)	(m^3/s)	(μg/L)	(μg)	(m^3)	-	-	-	-	-
0	113	1.423	77.4	0.00087	-3.42	0	154.8	0	-0.011	0	0	0
2	113	1.430	77.9	0.00091	-2.36	0	155.8	0.001	-0.008	-7.29034E-06	-6.74249E-09	-8.95308E-07
4	113	1.439	78.5	0.00096	-2.89	0	156.9	0.002	-0.010	-9.33639E-06	-1.76741E-08	-1.14025E-06
-	-	-	-	-	-	-		-	-	-	-	-
110	113	1.753	98.1	0.00205	848.68	208500	90.2	0.091	2.831	0.0061135	0.000558473	0.000413314
112	113	1.758	98.4	0.00206	859.76	212530	90.3	0.094	2.868	0.006232121	0.000582851	0.00041432
114	113	1.763	98.7	0.00207	874.54	217503	90.5	0.096	2.917	0.006378444	0.000610482	0.000416887
116	113	1.768	99.0	0.00209	859.23	214986	90.6	0.098	2.866	0.006305096	0.000617332	0.000405031
118	113	1.773	99.3	0.00210	850.26	214010	90.8	0.100	2.836	0.006276912	0.000628464	0.00039621
120	113	1.780	99.7	0.00211	879.82	223274	90.9	0.102	2.935	0.006533831	0.000668734	0.00040515
122	113	1.785	100.0	0.00213	955.03	243765	91.1	0.105	3.186	0.007150798	0.000747931	0.00043545
124	113	1.790	100.3	0.00214	955.55	245297	91.2	0.107	3.187	0.007196227	0.000768929	0.000430234
126	113	1.796	100.6	0.00215	991.97	256376	91.4	0.109	3.309	0.00751329	0.000819867	0.000440887
128	113	1.802	101.0	0.00217	992.76	258301	91.5	0.111	3.312	0.00757038	0.000843403	0.000435892
130	113	1.807	101.3	0.00218	975.61	255238	91.7	0.114	3.254	0.007489455	0.000851623	0.000423
132	113	1.811	101.5	0.00219	984.32	258641	91.8	0.116	3.283	0.007597985	0.000881546	0.000420814
134	113	1.818	101.9	0.00221	976.14	258431	92.0	0.118	3.256	0.007567743	0.000895626	0.000410901
136	113	1.822	102.1	0.00222	963.47	256165	92.1	0.121	3.214	0.007526038	0.000908314	0.000400465
138	113	1.828	102.4	0.00223	973.76	260542	92.3	0.123	3.248	0.007638867	0.000939895	0.000398223
140	113	1.833	102.7	0.00224	992.23	266869	92.4	0.125	3.310	0.007833093	0.000982331	0.000399927
142	113	1.839	103.1	0.00226	998.04	270093	92.6	0.128	3.329	0.007920025	0.001012074	0.000395895
144	113	1.844	103.4	0.00227	990.65	269460	92.7	0.130	3.305	0.007910068	0.001029736	0.000386976
-	-	-	-	-	-	-		-	-	-	-	-
1020	113	1.354	72.9	0.00020	179.4563	4392	99	1.040	0.599	0.000129597	0.000134737	6.1398E-05
1022	113	1.353	72.8	0.00018	179.9841	3815	99	1.040	0.600	0.000129978	0.000135162	6.16173E-05
1024	113	1.352	72.8	0.00014	179.4563	3106	99	1.040	0.599	0.000112234	0.000116731	5.32347E-05
1026	113	1.353	72.8	0.00018	178.1369	3776	98	1.040	0.594	9.09649E-05	9.4624E-05	4.31655E-05
1028	113	1.352	72.8	0.00014	176.5536	3056	98	1.040	0.589	0.000110419	0.000114881	5.24254E-05
1030	113	1.351	72.7	0.00010	181.0397	2216	98	1.041	0.604	9.24472E-05	9.61974E-05	4.39123E-05
1032	113	1.351	72.6	0.00014	181.5675	3029	98	1.041	0.606	6.55606E-05	6.82272E-05	3.1151E-05
1034	113	1.350	72.7	0.00000	178.4008	0	98	1.041	0.595	8.77985E-05	9.13825E-05	4.17351E-05
1036	113	1.351	72.7	0.00010	181.5675	2222	98	1.041	0.606	0	0	0
1038	113	1.351	72.7	0.00010	182.3591	2232	98	1.041	0.608	6.58465E-05	6.85415E-05	3.13101E-05
1040	113	1.351	72.7	0.00010	181.5675	2222	98	1.041	0.606	6.55606E-05	6.82511E-05	3.11839E-05
1042	113	1.351	72.7	0.00010	182.3591	2232	98	1.041	0.608	6.58465E-05	6.85558E-05	3.13297E-05
					∑	33892671				**0.998**	**0.35**	**0.07**
					M_{out} (g)	33.89267				**M_0***	**M_1***	**M_2***
					M_{in}(g)	40						
					Mass recovery %							
						85						

Figure 6.5: *Selected tracer study data from Experiment 1 and calculated parameters for volume-based RTD analysis.*

t	C(t)	C(t) x Δt	t x C(t) x Δt	t2 x C(t) x Δt
(min)	(µg/L)			
0	-3.42	-6.8373016	0.0000000	0.0000000
2	-2.36	-4.7261905	-9.4523810	-18.9047619
4	-2.89	-5.7817460	-23.1269841	-92.5079365
-	-			
110	848.68	1697.3571	186709.2857	20538021.4286
112	859.76	1719.5238	192586.6667	21569706.6667
114	874.54	1749.0794	199395.0476	22731035.4286
116	859.23	1718.4683	199342.3175	23123708.8254
118	850.26	1700.5238	200661.8095	23678093.5238
120	879.82	1759.6349	211156.1905	25338742.8571
122	955.03	1910.0516	233026.2937	28429207.8254
124	955.55	1911.1071	236977.2857	29385183.4286
126	991.97	1983.9405	249976.5000	31497039.0000
128	992.76	1985.5238	254147.0476	32530822.0952
130	975.61	1951.2183	253658.3730	32975588.4921
132	984.32	1968.6349	259859.8095	34301494.8571
134	976.14	1952.2738	261604.6905	35055028.5238
136	963.47	1926.9405	262063.9048	35640691.0476
138	973.76	1947.5238	268758.2857	37088643.4286
140	992.23	1984.4683	277825.5556	38895577.7778
142	998.04	1996.0794	283443.2698	40248944.3175
144	990.65	1981.3016	285307.4286	41084269.7143
-	-			
1020	179.4563492	358.9126984	366090.9524	373412771.4
1022	179.984127	359.968254	367887.5556	375981081.8
1024	179.4563492	358.9126984	367526.6032	376347241.7
1026	178.1369048	356.2738095	365536.9286	375040888.7
1028	176.5535714	353.1071429	362994.1429	373157978.9
1030	181.0396825	362.0793651	372941.746	384129998.4
1032	181.5674603	363.1349206	374755.2381	386747405.7
1034	178.4007937	356.8015873	368932.8413	381476557.9
1036	181.5674603	363.1349206	376207.7778	389751257.8
1038	182.359127	364.718254	378577.5476	392963494.4
1040	181.5674603	363.1349206	377660.3175	392766730.2
1042	182.359127	364.718254	380036.4206	395997950.3
	∑	279294.4841	112060550.2	69115714852
	t_m	**402**	**d**	**0.27**
	σ_c^2	**86482**	**N**	**1.86**
	σ_θ^2	**0.54**	P_e	**3.8**

Figure 6.6: *Selected tracer study data from Experiment 1 and calculated parameters for assumed steady-state MOM-analysis*

t	C(t)	TIS-model C(t)	SQE	LCF C(t) $_{F,P}$	SQE	LCF C(t) $_{F,F}$	SQE	LCF C(t) $_{P,P}$	SQE
0	-3.41865	0		0	11.68717325	0	11.68717325	0	11.68717325
2	-2.3631	1.988166429	18.93347809	0	5.584219104	0	5.584219104	0	5.584219104
4	-2.89087	7.691946321	111.9960651	0	8.357146794	0	8.357146794	0	8.357146794
-	-	-	-	-	-	-	-	-	-
110	848.6786	994.1411433	21159.35982	1029.781363	32798.22128	1698.68332	722508.0725	937.5	7889.246173
112	859.7619	996.8326173	18788.38025	993.9656374	18010.64184	1610.83826	564115.6916	921.0526316	3756.553194
114	874.5397	998.8940235	15464.00211	959.9864316	7301.146917	1528.947322	428249.3588	905.1724138	938.364224
116	859.2341	1000.343623	19911.88974	927.7202975	4690.355558	1452.514473	351981.5688	889.8305085	936.1385603
118	850.2619	1001.199816	22782.25308	897.0539877	2189.499027	1381.092453	281781.0713	875	611.973356
120	879.8175	1001.481096	14802.04024	867.8834603	142.4203566	1314.277274	188755.3296	860.6557377	367.1716135
122	955.0258	1001.205997	2132.611219	840.1129958	13204.95112	1251.703408	88017.60709	846.7741935	11718.40892
124	955.5536	1000.393056	2010.579414	813.6544106	20135.37184	1193.039588	56399.60817	833.3333333	14937.7866
126	991.9702	999.0607699	50.2756413	788.4263564	41430.11178	1137.985115	21320.3442	820.3125	29466.37905
128	992.7619	997.2275595	19.94207209	764.3536937	52170.31089	1086.266618	8743.131361	807.6923077	34250.75576
130	975.6091	994.9117382	372.5907988	741.366932	54869.40591	1037.635202	3847.23393	795.4545455	32455.67325
132	984.3175	992.13148	61.05890323	719.4017277	70180.34538	991.8639258	56.94914126	783.5820896	40294.68908
134	976.1369	988.9047921	163.0189482	698.3984333	77138.65851	948.7455791	750.2847237	772.0588235	41647.86324
136	963.4702	985.24949	474.3358133	678.301692	81321.09966	908.0907065	3066.892515	760.8695652	41047.03265
138	973.7619	981.1831741	55.07523849	659.0600726	99037.24316	869.7258598	10823.49865	750	50069.39002
140	992.2341	976.7232097	240.5885563	640.6257401	123628.4577	833.4920411	25199.04984	739.4366197	63906.57968
142	998.0397	971.8867081	683.9780746	622.9541581	140689.1506	799.2433179	39519.9946	729.1666667	72292.69866
144	990.6508	966.6905103	574.0951806	606.0038198	147953.2945	766.8455875	50088.7703	719.1780822	73697.43307
-	-	-	-	-	-	-	-	-	-
1020	179.4563	0.022134177	32196.63752	12.36742489	27918.70863	2.235701421	31407.158	102.739726	5885.440272
1022	179.9841	0.02149257	32386.54979	12.31916182	28111.54054	2.222627177	31599.15081	102.5390625	5997.738013
1024	179.4563	0.020869401	32197.09141	12.27118071	27950.88057	2.209654678	31416.39072	102.3391813	5947.057588
1026	178.1369	0.020264146	31725.53766	12.22347937	27527.26473	2.196782935	30954.92647	102.1400778	5775.517705
1028	176.5536	0.019676295	31164.21613	12.17605563	27019.9677	2.184010974	30404.74361	101.9417476	5566.924259
1030	181.0397	0.019105353	32768.44936	12.12890735	28530.84997	2.171337828	31993.88474	101.744186	6287.775764
1032	181.5675	0.018550838	32960.00653	12.08203239	28725.31028	2.158762543	32187.48084	101.5473888	6403.211849
1034	178.4008	0.018012282	31820.41669	12.03542865	27677.43467	2.146284178	31065.65211	101.3513514	5936.616559
1036	181.5675	0.01748923	32960.392	11.98909403	28756.82231	2.1339018	32196.40192	101.1560694	6465.991795
1038	182.3591	0.01698124	33248.65811	11.94302646	29041.64732	2.121614488	32485.56091	100.9615385	6625.567417
1040	181.5675	0.016487883	32960.75559	11.89722391	28787.98912	2.109421331	32205.18776	100.7677543	6528.592489
1042	182.3591	0.01600874	33249.01277	11.85168434	29072.788	2.09732143	32494.31854	100.5747126	6688.690429
		Sum SQE	**10540874.82**		**21155973.02**		**55337050.62**		**11299913.32**
		SOLVER τ (per N)	**65**	**SOLVER τ**	**173**	**SOLVER τ**	**176**	**SOLVER τ**	**205**
		N	**3.46**						
		Total τ	**225**						

Figure 6.7: *Selected tracer study data from Experiment 1, model data from TIS and LCF models and calculations for sum of squared errors with input mean residence time, τ, from Excel SOLVER function.*